Chapter One
Introduction

1.1 Introduction

The prefix nano in the word nanotechnology means a billionth (1×10^{9}) [1]. Nanotechnology deals with natural and artificial structures on the nanometer scale [2]. While the word *nanotechnology* is relatively new, the existence of functional devices and structures of nanometer dimensions is not new, and in fact such structures have existed on Earth as long as life itself [1]. Its infuse scientific branches from biology, chemistry, physics and engineering, hence called interdisciplinary subject opens new doors of applications[3]. It is important to distinguish here between 'nanoscience' and 'nanotechnology', nanoscience is the study of phenomena and manipulation of materials at atomic, molecular and macromolecular scales, where properties differ significantly from those at larger scale ,while the nanotechnologies are the design, characterization, production and application of structures, devices and systems by controlling shape and size at nanometer scale [4,5].Different properties can be obtained for the same material with different production methods, and the properties of the materials can be changed through thermal processes applied after production. The properties are characterized by color and brightness in terms of macro scale, while in micro scale, the particles affect all mechanical, physical and chemical properties and in the nano scale they represent atomic dimensions [2].

Nano materials/nano objects are materials that have one or more nano-sized external dimensions [2,6].The nano scale is the last step of the material before the atom. If all three dimensions of the material are less than 100 nm, such materials are called nano particles, quantum dots, nanoshells, nanorings and nanocapsules; if only two dimensions are less than 100 nm, they are called nanotube, nanowire and fiber; if only one dimension is less than 100 nm, it is called thin film, layer and coating. Optical, mechanical, electrical and color properties of the same material in macro/micro and nano size may be different or even the opposite of other scales[7].Some properties that do not occur in

macro size may appear in nano size.The main reason for this is the increased surface area/volume ratio with decreased material size and the non-continuous dimensions in nano-scale compared to macro dimensions [8,9,10].As the surface area/volume ratio increases, materials with low molecular weight can be formed [9,10] .

Although a few scientists had done related work earlier, nanotechnology didn't really get going until the second half of the twentieth century[11].The concepts that seeded nanotechnology were first discussed in 1959 by renowned physicist Richard Feynman in his talk *There's Plenty of Room at the Bottom*, in which he described the possibility of synthesis via direct manipulation of atoms. In 1960, Egyptian engineer Mohamed Atalla and Korean engineer Dawon Kahng at Bell Labs fabricated the

first MOSFET (metal–oxide–semiconductor field-effect transistor) with a gate oxide thickness of 100 nm, along with a gate length of 20 μm [12]. In 1962, Atalla and Kahng fabricated a nanolayer- Base metal- semiconductor junction (M-S junction) transistor that used gold(Au) thin films with a thickness of 10 nm[13]. The word "nanotechnology" was introduced for the first time into a scientific world by N. Taniguchi at the international conference on industrial production in Tokyo in 1974 in order to describe the superthin processing of materials with nanometer accuracy and the creation of nano-sized mechanisms [14]. Feynman put forward two other themes in his lecture. First, he had envisaged the possibility of making machines that could pick up and place single atoms to make chemical compounds. In 1981, Binnig and Rohrer, at IBM in Zurich, invented the scanning probe microscope. This uses a very sharp metal point scanned over a surface to 'see' the atoms in the surface. Eigler used the scanning probe microscope to 'nudge' atoms of xenon on a copper surface held at a temperature close to absolute zero to spell out the letters 'IBM'. Eigler and his group have done some remarkable work, mainly using the technique to explore basic physical and quantum mechanical phenomena. Gimzewski at IBM has used similar techniques, but at room

temperature, to push single molecules around on surfaces. This kind of work with single atoms and molecules is called ‘extreme .

nanotechnology’. Feynman's second vision in 1959 was of a factory in which billions of very small machine tools were drilling and stamping myriad tiny mechanical parts, which would then be assembled into larger products [4]. Ideas of nanotechnological strategy, which were put forward by Feynman, were developed by E. Drexler in his book “Vehicles of creation: the arrival of the nanotechnology era” published in 1986[14].At the beginning of the 21st century, very important advances were made in the use of nanotechnology in fields such as medicine, biotechnology, and computer technology, aviation, energy use, space studies, materials and manufacturing[15].In the future, as nanotechnology will play a major role in the discovery of new components and in the development of existing technologies, it is inevitable that the indispensable place of this technology loft will remain for many years [15].

Electricity and magnetism are very complex concepts, which have fascinated people for hundred of year [16]. They play a very important role in our lives. Due to their magnetic properties, magnets are offered by industries for various uses for example computers, MRI machines, toys, credit cards, etc [17]. Electricity is used for lighting rooms, working fans and domestic appliances like using electronic stoves etc [18].

Gum Arabic derived from exudates of Acacia Senegal and Acacia Sayal trees which are known to grow in the sub-Sahara region of the Sudan [19, 20]. The use of Arabic Gums dates back to the second millennium BC by Egyptians who used them as adhesives and ink stabilizers [21]. Today, the properties and features of GA have been widely explored and developed and it is being used in a wide range of industrial sectors such as textiles, ceramics, lithography, cosmetics and pharmaceuticals, encapsulation, food, etc [22].

1.2 Research Problem

Gum Arabic is one of the local materials which can be used in electronic thus one needs intensive research to show out the possibility it in manufacturing of electronic circuits, optical sensor and solar cells.

1.3 Aim of the Study

The aim of this work is to dope Talha and Hashab Gum Arabic with iodine to study their optical, electrical and structure properties.

1 .4 Layout of Study

The research consist of five chapter as follows: Chapter one is the introduction and proposal, Chapter two consist of the theoretical background Chapter three is the literature review, and then Chapter four is devote for the practical and methodology. Then the last chapter is concerned with analysis, discussion and conclusion.

Chapter Two

Theoretical Background

2.1Introduction

The study of Gum Arabic Talha and Hashab optical and electrical properties when doped with iodine need adequate theoretical background . This needs exihibiting optical and electrical properties of matter as well as the atomic structure of the talha , hahab and iodine.

2.2Atomic Structure

Atomic structure refers to the structure of atom comprising a nucleus (center) in which the protons (positively charged) and neutrons (neutral) are present. The negatively charged particles called electrons revolve around the center of the nucleus in fig. (2.1) [23].

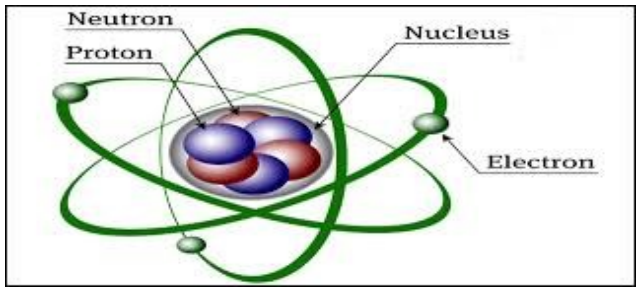

Figure (2.1) the structure of atom.

The history of atomic structure and quantum mechanics dates back to the times of Democritus, the man who first proposed that matter is composed of atoms [1]. Dalton was only partially correct about the particles that make up matter. While atoms cannot be broken down further by ordinary chemical or physical processes, they are composed of three smaller subatomic particles. The first clue about the subatomic structure came at the end of the 19th century when J.J. Thomson discovered the electron. Scientists knew that the overall charge of an atom was neutral, but Thomson's "plum pudding model"

of the atom attempted to reconcile this new information regarding the existence of a negatively-charged particle, suggesting that electrons were found studded throughout an area of positive charge. Just a few years later, Ernest Rutherford performed an experiment showing that most of an atom's mass is concentrated in the nucleus, where protons account for an atom's positive charge, and the tiny negatively-charged electrons make up most of the space outside of the nucleus. This disproved Thomson's plum pudding model and brought scientists one step closer to the familiar model of the atom we know today. The neutron was discovered later, in 1932, by James Chadwick. This final piece of the puzzle meant that scientists had now accounted for all the mass present in an atom with protons and neutrons, and all of its charge with protons and electrons [24].

2.3 Crystal Structure

Most solids are crystalline with their atoms arranged in a regular manner. They have what is called ***long-range order*** because the regularity can extend throughout the crystal. In contrast to this, amorphous materials such as glass and wax lack long-range order, but they have what is called ***short-range order*** so the local environment of each atom is similar to that of other equivalent atoms.

A crystal structure is formed by associating with a lattice a regular arrangement of atoms or molecules. In three dimensions there are three lattice constants, *a, b,* and c, and three angles: α(between *b* and c; *β* between *a* and c, and *γ* between lattice constants *a* and *b* There are 14 Bravais lattices, ranging from the lowest-symmetry triclinic type in which all three lattice constants and all three angles differ from each other *(a # b #* c and α # *β* # *γ),* to the highest-symmetry cubic case in which all the lattice constants are equal and all the angles are 90" *(a = b =* c and α= *β*= *γ* = 90"). There are three Bravais lattices in the cubic system, namely, a primitive or simple cubic (SC) lattice in which the atoms occupy the eight apices of the cubic unit cell, as shown in Fig. 2.1a, a body-centered cubic (BCC) lattice with lattice points

occupied at the apices and in the center of the unit cell, as indicated in Fig. 2.1b, and a face-centered cubic (FCC) Bravais lattice with atoms at the apices and in the centers of the faces, as shown in Fig. 2 .1 c [1].

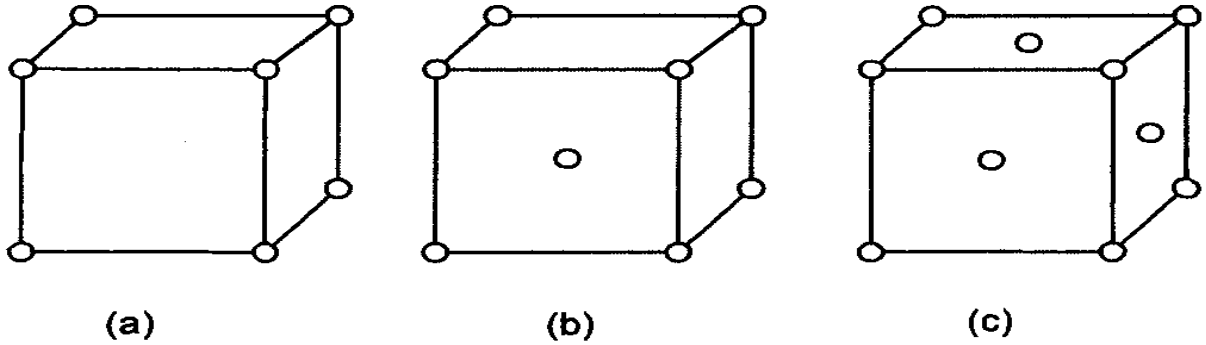

Figure (2.2) Unit cells of the three cubic Bravais lattices: (a) simple cubic (SC); (b) body-centered cubic (BCC); (c) face-centered cubic (FCC).

2.4 Optical Properties

2.4.1 Absorption

The absorption of light by an optical medium is quantified by its absorption coefficient *α.* This is defined as the fraction of the power absorbed in a unit length of the medium. If the beam is propagating in the x direction, and the intensity (optical power per unit area) at position x is 1 *(x),* then the decrease of the intensity in an incremental slice of thickness *dx* is given by:

$$dI = -\alpha dx \times I(x) \qquad (2.1)$$

This can be integrated to obtain Beer's law:

$$I_T = I_o e^{-\alpha x} \qquad (2.2)$$

Where I_0 is the optical intensity at x = 0. The absorption coefficient is a strong function of frequency, so that optical materials may absorb one color but not another [25].

2.4.2 Transmission

The phenomena of absorption, reflection, and transmission may be applied to the passage of light through a transparent solid. For an incident beam of

intensity I_0 that impinges on the front surface of a specimen of thickness l and absorption coefficient, the transmitted intensity at the back face I_T is

$$I_T = I_o(1 - R)^2 e^{-\alpha l} \quad (2.3)$$

Where R is the reflectance; for this expression, it is assumed that the same medium exists outside both front and back faces. The derivation of Equation (2.2) is left as a homework problem. Thus, the fraction of incident light that is transmitted through a transparent material depends on the losses that are incurred by absorption and reflection. Again, the sum of the reflectivity R, absorptive A, and transmissivity T, is unity according to Equation (2.3). Also, each of the variables R, A, and T depends on light wavelength. This is demonstrated the transmission [26].

2.4.3 Reflection

When light radiation passes from one medium into another having a different index of refraction, some of the light is scattered at the interface between the two media even if both are transparent. The reflectivity R represents the fraction of the incident light that is reflected at the interface, or

$$R = \frac{I_R}{I_o} \quad (2.4)$$

Where I_0 and I_R are the intensities of the incident and reflected beams respectively. If the light is normal (or perpendicular) to the interface, then

$$R = \left(\frac{n_2 - n_1}{n_{2+} n_1}\right)^2 \quad (2.5)$$

Where n_1 and n_2 are the indices of refraction of the two media. If the incident light is not normal to the interface, R will depend on the angle of incidence. When light is transmitted from a vacuum or air into a solid s, then

$$R = \left(\frac{n_s - 1}{n_s + 1}\right)^2 \quad (2.6)$$

Because the index of refraction of air is very nearly unity. Thus, the higher the index of refraction of the solid, the greater the reflectivity [25, 26].

2.4.4 Absorption Coefficients

Much of the information about the properties of materials is obtained when they interact with electromagnetic radiation. When a beam of light (photons) is incident on a material, the intensity is expressed by the Lambert-Beer-Bouguer law as Equation (2.2). If this condition for absorption is met, it appears that the optical intensity of the light wave, (I), is exponentially reduced while traveling through the film. If the power that is coupled into the film is denoted by I_0, gives the transmitted intensity that leaves the film of thickness d.(α) Is called "absorption coefficient". From Equation (2.2) it follows that

$$\alpha = -\frac{1}{d}\,\mathrm{Lin}\left(\frac{I}{I_o}\right) \qquad (2.7)$$

It is clear that α must be a strong function of the energy hν of the photons. For $h\nu < E_g$ (direct), no electron hole pairs can be created, the material is transparent and α is small. For $h\nu \geq E_g$ (direct), absorption should be strong. All mechanisms other than the fundamental absorption may add complications (e.g. "sub band gap absorption" through excitons), but usually are not very pronounced. Optical transmission measurements were carried out to determine the film thickness, the wavelength dependence of the refractive index and optical absorption coefficient. The optical constants were determined from the optical transmission measurements using the method described by Swanepoel.

The transparent substrate has a thickness several orders of magnitude larger than (d) and has index of refraction (n) and absorption coefficient (α = 0). The index of refraction for air is taken to be n_0 =1. In the transparent region (α =0) the transmission is determined by n and s through multiple reflections. In the region of weak absorption α is small and the transmission begins to decrease. In the medium absorption region α is large and the transmission decreases

mainly due to the effect of α. In the region of strong absorption, the transmission decreases drastically due almost exclusively to the influence of α. If the thickness d is uniform, interference effects give rise to the spectrum [26].

2.4.5 Determination of Band Gaps

The fundamental absorption is related to band-to-band or to exaction transition, which are subjected to certain selection rules. The transitions are classified into several types, according to the band structure of a material. The relation between absorption coefficient and optic band gap for direct transition (k=0) is given by Tauc equation:

$$\sqrt{\alpha h\nu} = B(h\nu - E_g^{opt}) \quad (2.8)$$

And for indirect transition (k ≠ 0) the relation becomes

$$\alpha(h\omega) \propto \frac{(\hbar\omega - E_{gap})^2}{\hbar\omega} \quad (2.9)$$

From the αhν versus hν one obtains E_g and B parameters. B is also a useful diagnostic of the material since it is inversely proportional to the extent of the tail state (Δ E) at conduction and valance band edges [26].

2.4.6 Refractive Index

The propagation of the beam through a transparent medium is described by the refractive index *n.* This is defined as the ratio of the velocity of light in free space c to the velocity of light in the medium *v* according to [27]:

$$n = \frac{c}{\upsilon} \quad (2.10)$$

The magnitude of n (or the degree of bending) will depend on the wavelength of the light. This effect is graphically demonstrated by the familiar dispersion or se parathion of a beam of white light into its component colors by a glass prism. Each color is deflected by a different amount as it passes into and out of the glass, which results in the separation of the colors. Not only does the index of refraction affect the optical path of light, but also, as explained shortly, it influences the fraction of incident light that is reflected at the

surface. Just as Equation (2.10) defines the magnitude of c, an equivalent expression gives the velocity of light in a medium as

$$\nu = \frac{1}{\sqrt{\varepsilon\mu}} \qquad (2.11)$$

Where ε and μ are respectively, the permittivity and permeability of the particular substance. From Equation (2.11), we have

$$n = \frac{c}{\nu} = \frac{\sqrt{\epsilon\mu}}{\sqrt{\epsilon_o\mu_o}} = \sqrt{\epsilon_r\,\mu_r} \qquad (2.12)$$

Where ϵ_r and μ_r are the dielectric constant and the relative magnetic permeability, respectively. Because most substances are only slightly magnetic, and

$$n \cong \sqrt{\epsilon_r} \qquad (2.13)$$

Thus, for transparent materials, there is a relation between the index of refraction and the dielectric constant [26].

2.4.7The Complex Refractive Index and Dielectric Constants

In general, the difference in the propagation of an electromagnetic wave through vacuum and some other material can be described by a complex refractive index, n:

$$\tilde{n} = n + ik \qquad (2.14)$$

The real part of $\tilde{n}$, namely *n,* is the same as the normal refractive index defined in eqn. 2.10. The imaginary part of $\tilde{n}$, namely *K,* is called the extinction coefficient. For transparent materials it is purely real, the imaginary part being related to the *absorption coefficient* by:

$$\alpha = \frac{2kw}{c} = \frac{4\pi k}{\lambda} \qquad (2.15)$$

However, when performing calculations of optical properties it is common to evaluate the complex dielectric constant and then express other properties in terms of it. The complex dielectric constantϵ_r is given by:

$$\epsilon_r = \epsilon_1 + i\epsilon_2 \quad (2.16)$$

By analogy with eqn. 2.13, we see that $\tilde{n}$ and ϵ are related to each other through:

$$\tilde{n}^2 = \epsilon_r \quad (2.17)$$

We can now work out explicit relationships between the real and imaginary parts of n and ε by combining eqns 2.14, 2.16 and 2.17. These are:

$$\epsilon_1 = n^2 - k^2 \quad (2.18)$$

$$\epsilon_2 = 2nk \quad (2.19)$$

Where the real the dielectric constants (ε_1),and the imaginary the dielectric constant (ε_2) [28].

2.5 Magnetic Properties

2.5.1 Magnetic Flux Density and Intensity

The magnetic flux density is defined as the total number of lines of magnetic force, which emanates from the north pole of magnet. If $\emptyset$ is the amount of flux which passes through a given area of cross-section A, then the magnetic flux density is defined by the expression [29]

$$\mathrm{B} = \frac{\emptyset}{\mathrm{A}} \quad (2.20)$$

The magnetic field strength and flux density are related according to

$$B = \mu_0 H \quad (2.21)$$

The parameter μ_0 is the magnetic permeability of free space and has a value $4\pi \times 10^{-7}\ N/Amp^2$ .The unit *of magnetic field are* Amper/meter.If the system is surrounded by material medium then

$$B = \mu H \tag{2.22}$$

Where μ is the magnetic permeability of the medium .Its related to μ_0 by

$$\mu = \mu_r\, \mu_0$$

$$\mu_r = \frac{\mu}{\mu_0} \tag{2.23}$$

Where μ_r is called the *relative permeability,* which is unitless. In matter, we have

$$B = \mu_0 H + \mu_0 M$$

The magnetization *M is defined as magnetic moment per unit volume. It is* proportional to the magnetic field intensity H.

$$M = \mu \frac{N}{V}$$

$$M = x_m H \tag{2.24}$$

Where x_m is called the magnetic susceptibility. If the χ is negative, the solid is called diamagnetic, and if it is positive, the solid is called paramagnetic. The magnetic susceptibility and the relative permeability are related as follows [30, 31].

$$x_m = \mu_r - 1 \tag{2.25}$$

2.5.2 The Biot-Savart Law

The equation used to calculate the magnetic field produced by a current is known as the Biot-Savart law. This law enables us to calculate the magnitude and direction of the magnetic field produced by a current in a wire. The **Biot-Savart law** states that at any point *P* [Fig (2.3)], the magnetic field $d\vec{B}$ due to an element $d\vec{I}$ of a current-carrying wire is given by

$$d\vec{B} = \frac{\mu_0}{4\pi} \frac{Id\vec{l} \times \hat{r}}{r^2} \tag{2.26}$$

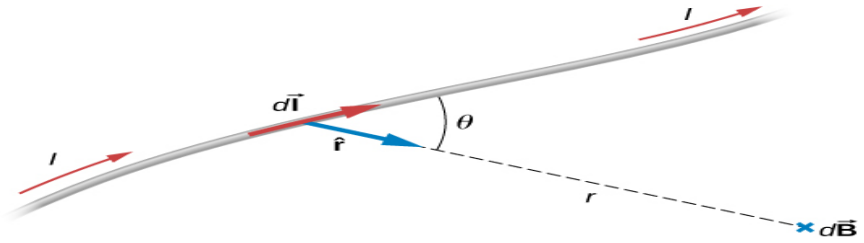

Figure (2.3) The Biot-Savart law.

The infinitesimal wire segment $d\vec{I}$is in the same direction as the current I (assumed positive), r is the distance from $d\vec{I}$ to P and $\hat{r}$ is a unit vector that points from $d\vec{I}$ to P, as shown in the figure. The direction of $d\vec{B}$ is determined by applying the right-hand rule to the vector product $d\vec{I} \times \hat{r}$. The magnitude of d $\vec{B}$ is

$$d\vec{B} = \frac{\mu_0}{4\pi}\frac{Idl\sin\theta}{r^2} \qquad (2.27)$$

Where θ is the angle between $d\vec{I}$ and $\hat{r}$. Notice that if $\theta = 0$, then $d\vec{B} = 0$. The field produced by a current element I$d\vec{I}$ has no component parallel to $d\vec{I}$. The magnetic field due to a finite length of current-carrying wire is found by integrating equation 2.27 along the wire, giving us the usual form of the Biot-Savart law [32].

The magnetic field $\vec{B}$ due to an element $d\vec{I}$ of a current-carrying wire is given by

$$\vec{B} = \frac{\mu_0}{4\pi}\int_{wire}\frac{IdI\times\hat{r}}{r^2} \qquad (2.28)$$

2.5.3 Amper Law

Ampere's law physical law that states that the line integral of the magnetic field around an electric current is proportional to the current [25].It can be written

$$\oint \vec{B}.\overrightarrow{ds} = \mu_0 i_{enc} \quad (Amper\ law) \qquad (2.29)$$

The line integral in this equation is evaluated around a closed loop called an Amperian loop. The current i on the right side is the net current encircled by the loop. The current i_{enc} is the *net* current encircled by that closed loop[33].

$$i_{enc} = i_2 - i_1$$

2.5.4 Magnetic Dipole Moment

Consider a charge particle moving in a circular orbit in fig(2.4) (an electron around a nucleus).The magnetic moment is given by

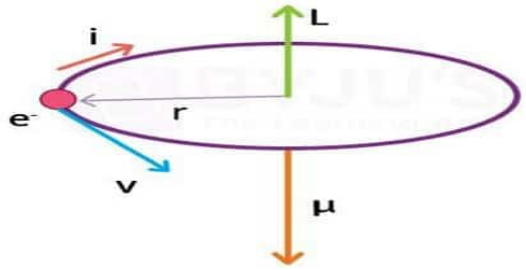

Figure (2.4) Angular momentum vector of electron producing current.

$$\mu_m = IA \qquad (2.30)$$

Here I is the current and A is the area of the loop. Let us now relate the magnetic moment to the angular momentum of the electron. If the angular velocity of the electron is ω, then the loop current becomes

$$I = -e(\frac{\omega}{2\pi}) \qquad (2.31)$$

Since we know the relationship between the current loop and the area of the loop. The magnetic dipole moment expression can be calculated as

$$\mu_m = -\left(\frac{e}{2m}\right)(m\omega r^2)$$

$$\mu_m = -\left(\frac{e}{2m}\right)(L) \qquad (2.32)$$

Here L= $m\omega r^2$ is the angular momentum of the electron. The minus signin eq. 2.32 indicates that the dipole moment points in a direction opposite to vector representing the angular momentum [29].

The magnitude of the orbital angular momentum L of the electrons is quantized in terms of $\hbar$

$$L = \hbar\sqrt{l(l+1)}$$

$$\mu_m = -\left(\frac{e}{2m}\right)(L) = \frac{e\hbar}{2m}\sqrt{l(l+1)} = \mu_B\sqrt{l(l+1)}$$

Where $\mu_B = \frac{e\hbar}{2m} = 9.27 \times 10^{-24} \quad J/T,$ which is called the Bohr magenton [34].

Electron also has spin rotation about their own axis. Thus, there is a magnetic moment associated with the spin, and this moment may be related to the spin angular momentum by the relationship

$$\mu_s = \left(-\frac{e}{m}\right) S \qquad (2.33)$$

This shows that the spin gyromagnetic ratio $\left(-\frac{e}{m}\right)$ is twice the value obtained for the orbital motion [29].

2.5.5 Types of Magnetic Materials

Magnetic materials can be classified according to how they react to the application of magnetic field.

1. Ferromagnetic materials the atoms have permanent magnetic moments that align readily with an externally applied magnetic field. Examples of Ferromagnetic materials are iron, cobalt, and nickel. Such substances can retain some of their magnetization even after the applied magnetic field is removed.
2. Paramagnetic materials also have magnetic moments that tend to align with an externally magnetic field, but the response is extremely weak compared with that of Ferromagnetic materials. Examples of Paramagnetic substances are aluminum, calcium, and platinum.
3. Diamagnetic materials an externally applied magnetic field induces a very weak magnetization that opposite the applied field. Ordinarily diamagnetism isn't observed because paramagnetic and ferromagnetic effects are far stronger [35].

2.5.6 Langevins Theory of Diamagnetic

Diamagnetism is inherent in all substances and arises out of the effect of a magnetic field on the motion of the electron in an atom. Suppose an electron is revolving around the nucleus in atom the force between electron and nucleus is

$$F_C = mr{\omega_0}^2 \quad (2.34)$$

When this atom is subjected to a magnetic field, electron also experiences an additional force called Lorentz force

$$F_L = -er\omega B \quad (2.35)$$

Equation (2.34) thus becomes

$$F_c - er\omega B = mr\omega^2 \quad (2.36)$$

Substituting F_c from equation 2.34 and solving for ω, we get

$$\omega = \pm\omega_0 - \frac{eB}{2m} \quad (2.37)$$

Substituting the value of Larmors frequency ($\omega_l = \frac{eB}{2m}$)we get

$$\omega = \pm\omega_0 - \omega_L \quad (2.38)$$

Thus the change in magnetic moment is

$$\Delta\mu_m = -\left(\frac{e^2 r^2}{4m}\right) B \quad (2.39)$$

If there are Z numbers of electrons in an atom, the total induced moment in the atom is given by the expression

$$\Delta\mu_m = -\frac{Z e^2}{4m} B\langle r^2\rangle \quad (2.40)$$

Where $\langle r^2\rangle$is the mean square radius of the projection of the orbit on a plane perpendicular to magnetic field axis. If the coordinates of a point of orbit of radius $r_0$are x, y, z then the mean square radius in this case becomes

$$\langle {r_0}^2\rangle = x^2 + y^2 + z^2$$

For spherical symmetry

$$\langle x^2\rangle = \langle y^2\rangle = \langle z^2\rangle$$

Therefore

$$\langle r^2 \rangle = \langle x^2 \rangle + \langle y^2 \rangle = \langle 2x^2 \rangle$$

$$\langle r^2 \rangle = \frac{2}{3} {r_0}^2 \qquad (2.41)$$

Substituting $\langle r^2 \rangle$ in equation (2.40), we get the expression for total induced moment in the atom as

$$\Delta\mu_m = -\frac{Z\, e^2 B {r_0}^2}{6m} \qquad (2.42)$$

If there are n atoms per unit volume, the magnetization produced would be

$$M = n\Delta\mu_m = -\frac{nZe^2\, {r_0}^2}{6m} B$$

$$M = \frac{nZe^2\, {r_0}^2}{6m} \mu H \qquad (2.43)$$

The diamagnetic susceptibility χ is therefore given by

$$\chi_{dia} = -\frac{nZe^2\, {r_0}^2}{6m} \mu \qquad (2.44)$$

Equation 2.44 is classical expression deduced by Langevin for explaining the theory of diamagnetic [29].

2.5.7 Longevin s Theory of Paramagnetism

Consider a material with **N** magnetic dipoles per unit volume, each with moment μ_m**.** In the presence of a magnetic field B, the potential energy of magnetic dipole

$$V = -\mu_m B \cos\theta$$

$$V = -\mu_m . B \qquad (2.45)$$

Here θ is the angle between the magnetic moment and the field. Now, in absence of thermal agitation, each permanent magnetic dipole will become oriented in such way that is potential energy minimized. With all the dipoles lined up, the magnetization is given by

$$M = N\mu_m L(a) \qquad (2.46)$$

Here L(a) is known as the Langevins function ,where

$$a = \frac{\mu_m B}{kT}$$

$$L(a) = \coth a - \frac{1}{a} \qquad (2.47)$$

Langevins function is mathematical function, which is relevant to the theory of paramagnetism. A plot of Langevins function is shown in fig (2.5).

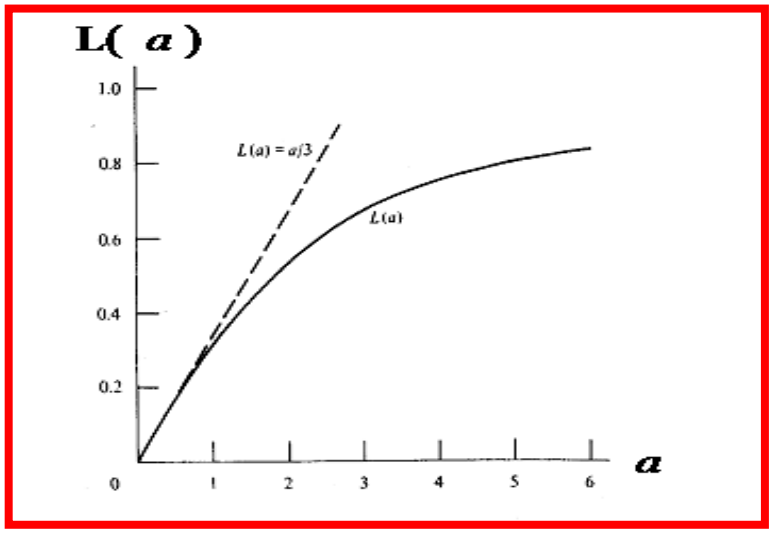

Figure (2.5) Plot of Langevins function.

If$a \ll 1$, the function L (a) may be appointed as $L(a) = \frac{a}{3}$ .The expression for magnetization thus becomes

$$M = \frac{N\ {\mu_m}^2\ B}{3k\ T}$$

$$\frac{M}{H} = \chi_p = \frac{N\mu_0\ {\mu_m}^2}{3\ kT} \qquad (2.48)$$

This is known as the "Curie Law". The susceptibility χ_p is referred as the Langevin paramagnetic susceptibility. It can be written in a simplified form as

$$\chi_p = \frac{C}{T} \qquad (2.49)$$

$Where\ C = \frac{N\mu_0\ {\mu_m}^2}{3k}$ $is\ known\ as\ the\ curie\ constant$ .The varation of paramagnetic susceptibility with temperature is shown in fig.(2.6) [29].

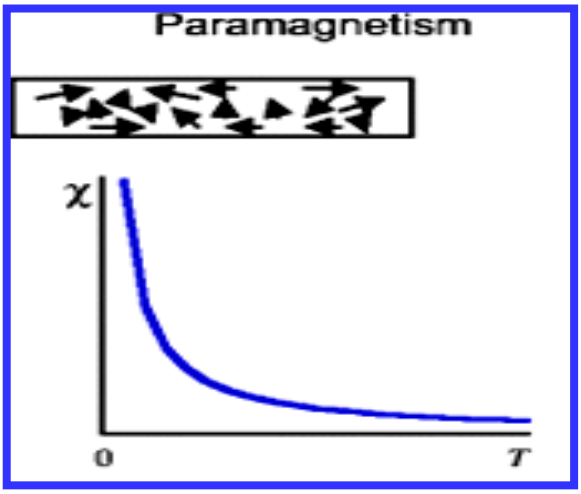

Figure (2.6) Paramagnetic Susceptibility Curve (Curie Law).

2.5.8 Quantum Mechanical Expression for Paramagnetism

The magnetization is given by

$$M = Ng\mu_B J B_z(\acute{a}) \tag{2.50}$$

Where N is the number of atoms per unit volume, g the g factor, $\mu_B$the Bohr magneton and $B_{Z(\acute{a})}$is called the Brillouin function for low magnetic field and /or high temperature

$$B_{z(a)} = \left(\frac{J+1}{3J}\right)\acute{a}$$

$$M = Ng\mu_B J\left(\frac{J+1}{3J}\right)\left(\frac{g\,\mu_B\, JH}{k_B\, T}\right)$$

$$M = \frac{Ng^2{\mu_B}^2 J(J+1)H}{3k_B T} \tag{2.51}$$

Therefore

$$\chi_P = \frac{M}{\mu_0 H} = \frac{Ng^2{\mu_B}^2 J(J+1)}{3\mu_0 k_B} = \frac{C}{T} \tag{2.52}$$

This is the Curie law for quantum-mechanical magnetic moments [36].

Where the curie constant $C = \frac{Ng^2{\mu_B}^2 J(J+1)}{3\mu_0 k_B}$

2.6 Electrical Properties:

2.6.1 Electrical Conductivity

Electrical conductivity is the ratio of the current density to the electrical field strength. Also, the greater the value of the conductivity, the lower the resistance it provides to the flow of electric current.

$$\sigma = \frac{J}{E} \tag{2.53}$$

The conductivity formula is the inverse of the resistivity that is:

$$\sigma = \frac{1}{\rho} \tag{2.54}$$

$$\rho = \frac{1}{\sigma} = \frac{E}{J} \tag{2.55}$$

Where E is the magnitude of the applied electric field. The SI unit of resistivity is the ohm-meter (Ω.m). Equation 2.55 corresponds to the vector equation

$$\vec{E} = \rho\vec{J} \tag{2.56}$$

If we know the resistivity of a substance such as copper, we can calculate the resistance of a length of wire made of that substance. Let A be the cross-sectional area of the wire, let L be its length, and let a potential difference V exist between its ends [Fig. (2.7)].

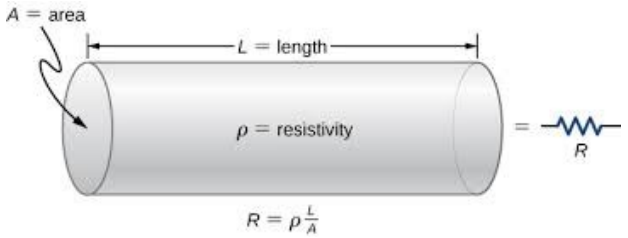

Figure (2.7**)** a potential difference applied to a segment of a conductor with a cross-sectional area *A and a length L*.

From equation (2.55)

$$\rho = \frac{E}{J} = \frac{V/L}{i/A} \tag{2.57}$$

However, V/i is the resistance R,

$$R = \frac{\rho L}{A} \quad (2.58)$$

The resistance of a given material is proportional to the length, but inversely proportional to the cross-sectional area [34].

2.6.2 Electric Permittivity

The electric flux density **D** resulting from an applied electric field **E** is

$$D = \varepsilon E \quad (2.59)$$

Here, ε is the constant of proportionality, and it is called. "Permittivity". The permittivity of a medium is expressed as the product of the dielectric constant and the free space permittivity

$$\varepsilon = \varepsilon_r \varepsilon_0$$

$$\varepsilon_r = \frac{\varepsilon}{\varepsilon_0} \quad (2.60)$$

Relative permittivity is directly related to electric susceptibility χ_e by

$$\chi_e = \varepsilon_r - 1$$

Otherwise written as

$$\varepsilon = \varepsilon_r \varepsilon_0 = (1 + \chi_e)\varepsilon_0 \quad (2.61)$$

The electric displacement **D** is related to the polarization density **P** by

$$D = \varepsilon_0 E + P \quad (2.62)$$

Using equations 2.59 and 2.62 we get

$$\varepsilon E = \varepsilon_0 E + P$$
$$(\varepsilon - \varepsilon_0)E = P = (\varepsilon_0 \varepsilon_r - \varepsilon_0)E$$
$$p = (\varepsilon_r - 1)\varepsilon_0 E$$

Therefore the polarization can be written

$$p = \varepsilon_0 \chi_e E \quad (2.63)$$

The polarization is proportional to the total electric flux density and electric field [37, 38].

2.7 Nanomaterial

Nanomaterials are materials that have structural components smaller than 1 μm in at least one dimension. While the atomic and molecular building blocks (□ 0.2 nm) of matter are considered nanomaterials, examples such as bulk crystals with lattice spacing of nanometers but macroscopic dimensions over all are commonly excluded *[39]*. It's having been intentionally designed for industrial applications. They can be applied in cell phones, CD-ROMs, magnetic recordings, cosmetics, drug delivery in medicine, imaging, water splitting etc. Its include ultrathin films, quantum wire, and nanoparticles-quantum dots, in general [40]. There are two process for nanomaterial creation including "bottom-up" processes (such as self-assembly) that create nanoscale materials from atoms and molecules, and "top-down" processes (such as milling) that create nanoscale materials from their macro-scale counterparts. Nanoscale materials that have macro-scale counterparts frequently display different or enhanced properties compared to the macro-scale form. Such engineered or manufactured nanomaterials will be referred to as "intentionally produced nanomaterials, or simply "nonmaterial's [41].

2.7.1 Sources of Nanomaterials

Sources of nanomaterials can be classified into three main categories based on their origin: incidental nanomaterials,; engineered nanomaterials, and naturally produced nanomaterials *[42]*.

2.7.2 Type of Nanmaterial's

2.7.2.1 Carbon-Based Nanomaterials

These nanomaterials are composed mostly of carbon, most commonly taking the form of a hollow spheres, ellipsoids, or tubes. These particles have many potential applications, including improved films and coatings, stronger and lighter materials, and applications in electronics[43].

2.7.2.2Metal-Based Nanomaterials

These nanomaterials include quantum dots, nanogold, nanosilver and metal oxides, such as titanium dioxide, zinc oxide, magnesium oxide, iron oxide etc[44].

2.7.2.3 Dendrimers

These nanomaterials are nanosized polymers built from branched units. The surface of a dendrimer has numerous chain ends[45].

2.7.2.4 Nanocomposites

Combine nanoparticles with other nanoparticles or with larger, bulk-type materials. Nanoparticles, such as nanosized clays, are already being added to products ranging from auto parts to packaging materials, to enhance mechanical, thermal, barrier, and flame-retardant properties [46].

2.8 Nanoparticle

Nanoparticles are generally defined as particulate matter with at least one dimension that is less than 100 nm. This definition puts them in a similar size domain as that of ultrafine particles (air borne particulates) and places them as a sub-set of colloidal particles [47].Its can have amorphous or crystalline form, and their surfaces can act as carriers for liquid droplets or gases[48].It's are currently made out of a very wide variety of materials, the most common of new generation of nanoparticles being ceramics, which are best split into metal oxide ceramics, such as titanium zinc , aluminum and iron oxides ,to name a prominent few, and silicate nanoparticles, generally in the form of nanoscale flakes of clay[49].

2.8.1 Production Techniques

There a wide variety of techniques for producing nanoparticles. These essentially fall into three categories condensation from vapor, chemical synthesis and solid state process such as milling [49].

2.8.2NanoparticleClassification

Nanoparticles are generally classified based on their dimensionality, morphology, composition, uniformity, and agglomeration.

A. Dimensionality

As shape, or morphology, of nanoparticles plays an important role in their toxicity, it is useful to classify them based on their number of dimensions .This is a generalization of the concept of aspect ratio *one-dimensional (1D) nanomaterials*, *two-dimensional (2D) nonmaterials* and *three-dimensional (3D) nanomaterials* [50].

B. Nanoparticle Morphology

Morphological characteristics to be taken into account are flatness, sphericity, and aspect ratio. A general classification exists between high- and low-aspect-ratio particles.

C. Nanoparticle Composition

Nanoparticles can be composed of a single constituent material or be a composite of several materials.

D. Nanoparticle Uniformity and Agglomeration

Based on their chemistry and electromagnetic properties, nanoparticles can exist as dispersed aerosols, as suspensions/ colloids, or in an agglomerate state [39].

2.9 Gum Arabic

Gum Arabic (GA) is a natural polymer [51]. It is a natural polysaccharide of high-molecular weight, mainly calcium, magnesium, and potassium salts and some mineral elements. It is a water soluble polysaccharide of the hydrocolloid group, on hydrolysis yield arabinose, galactose, rhamnose and glucuronic acid [52, 53].

2.9.1 Types of Gum Arabic:

There are three types of gum Arabic:

- Hashab gum Arabic, used in reducing the proportion of urea in the blood that lead to reduce the degree of kidney failure.
- Gum Talha, and is used in various industries as an industry colors, Cosmetics and otherwise.

- Gum rosin, and has other medical uses such as drugs for chest diseases [54].

2.9.2Chemical and Physical Properties of Gum Arabic:

2.9.2.1Solubility

Regarding to the solubility the true gums are divisible into three classes: 1) soluble gums that dissolve in water forming transparent solution e.g *Acacia Senegalgum*.

2) Insoluble gums which also absorb water but on addition of sufficient water break down into very thick transparent solution e.g tragacnth gum.

3) Half – soluble gums that partially dissolve but on addition of more water pass into soluble e.g. ghatti gum [55].

2.9.2.2Nitrogen

The role of nitrogen and nitrogenous component in the structure, physicochemical properties and functionality of gum Arabic was recently subjected to intensive investigation. On the other hand Erick Dickens (1991) studied the emulsifying behavior of gum and concluded that there was a strong correlation between the proportion of protein in the gum and it's emulsifying stability[55,56].

2.9.2.3Viscosity

The viscosity can be presented in many terms such as relative viscosity, specific viscosity, reduced viscosity, inherent viscosity and intrinsic viscosity. It is also presented as kinematical or dynamic viscosity; intrinsic viscosity was used to determine the molecular weight of *Acacia Senegal* gum.

2.9.2.4SpecificRotation:

The optical activity of organic molecules is related to their structure and is a characteristic property of the substance, and thus the specific rotation is considered as the most important criterion of purity and identity of any type of gum [57, 55].

2.9.2.5 Conductivity:

Conductivity is the ability, or power to transmit or conduct an electrical charge .To measure conductivity an electronic Conductivity meter is used. Many are combined with PH meter so that instruments can measure PH and conductivity at the same time [55].

2.9.2.6 Moisture

Moisture content determines the hardness of the gum and hence the variability of densities and the amount of air entrapped during nodule formation [55, 58].

2.10 Iodine

Iodine was discovered by chance at the beginning of the 19th century [59]. It occurs naturally as iodide salts in seaweeds, fish, and shell fish and also in seawater [60]. It has an atomic mass 126.9044, atomic number 53, atomic radius is 133.3 pm, a nonmetallic element of the halogen family, appears in group 17 of the periodic table between bromine and astatine. The electronic configuration of the iodine atom is [Kr] $4d^{10}5s^{2}5p^{5}$ [61, 62]. The two most common radioactive isotopes are iodine-129 and iodine-131 .The isotope of iodine in the environment that is most abundant naturally is iodine-127, but radioactive isotopes also occur naturally in the enviroment. Iodine-129 is produced naturally in the upper atmosphere when cosmic rays from the solar system hit the element xenon .Xenon degrades into this radioactive iodine and beta particles and gamma radiation [63].Iodine is used in various fields of science and technology including medicine [64].

2.11 Chemical and Physical properties of Iodine:

- Iodine as a solid, which is its normal form (at 25 ˚C and 1 atm), the color in its gaseous state is violet.
- Melting point is 113.7 ˚C and Boiling point is 184.4 ˚C.
- starch is a common indicator for the presence of iodine to change color [65].
- Iodine single crystals were semiconducting, it have photoconductivity properties [66].

- Iodine accepts electrons from the solvent molecule into its lowest unoccupied molecular orbital (LUMO) [67].

CHAPTER THREE
LITERATURE REVIEW

3.1 Introduction

Many attempts were made to use Gum Arabic in fabrication of solar cells and electronic circuit .The physical characteristics of these Gum Arabic like energy gap and absorption coefficient are important parameters that plays on important role in solar cells performance .In this chapter different attempts made will be exhibited here .

3.2 Improving the Properties of Gum Arabic to Act as Semiconductor

This work was done by H. Mustafa. In this work Gum Arabic was doped by iodine of different concentrations at room temperature (25^{o}C). The effect of vaccination of iodine on the distance between atoms and the angles between them was studied using Easy Scan device. In addition of determination the absorption and energy gap of the treated samples using (UV-VIS) spectroscopy. In Gum Talha the largest distance between atoms was 70.8 nm when concentration is 1.52mg/L and the distance smaller for 1.22mg / L In gum Hashab distance between atoms increases between (1.2 - 2.0) mg / L where 68.3nm then begin increasing. Were prepared solutions of gum Arabic and iodine concentrations certain were studied gap energy and higher wavelength was him absorbency in Gum Talha higher wavelength of absorbency is 360nm in gum Hashab 350 nm and found that the gap energy affected by a concentration of gum in Gum Talha when he the energy gap for 1 mg of Talha is 3.04 eV while for 2gm diluted with 5ml distilled water is 3.09 eV the energy gap. In Hashab gum 1g has gap energy 3.04eV, while when the concentration of gum is 2g the energy gap is 2.99 eV [68].

3.3 Effects of γ-Irradiation on Some Properties of Gum Arabic (Acacia Senegal)

The work done by Siddig T. Kafi studied the effect of γ radiation having different doses , on gum arabic (acacia Senegal).The gum Arabic samples were collected from Blue Nile state in Sudan at 2008. Doses of 5.5, 6.5, 7.5,

8.5, 9.5, and 10.5 KGy were used respectively for irradiation of gum Arabic samples. The properties studied include the emulsifying stability, viscosity and absorption. It was found that the best emulsifying stability, highest relative viscosity and highest absorbance were obtained with the highest radiation dose(10.5 KGy).Absorbance increased drastically compared with the control sample (not irradiated sample).Red shift in the peak absorption wavelength was also observed. Change in the colour of irradiated samples occurred from white to red color. Hence gamma radiation is capable of enhancement of the properties of gum Arabic material. It was found that the highest dose of gamma radiation used achieved the best emulsification, viscosity and absorbance. The only drawback is the change of the colour of gum Arabic from white to dark red [69].

3.4 Investigating the Electric Conductivity, Magnetic Inductivity, and Optical Properties of Gum Arabic Crystals

Elhadi M. I. Elzain was done his study on samples of Gum crystals of different thicknesses which were prepared by drying Gum solution. A special Capacitor was designed, to determine the electric permittivity. Investigations were carried out with special emphasis on the effects of temperature, crystal thickness, light intensity, upon the desired properties. The maximum value of electric permittivity is 2.8×10^{-4} C/Nm^2.The maximum value of electric conductivity is 9.88×10^{-7} ohm-1 cm^{-1}. The results indicated that; Gum Arabic crystals could be considered as large band gap semiconductor. The light intensity has slight effect on the conductivity, permittivity, and the current passing through the crystals. The electrical properties of gum Arabic indicate that; its behavior resembles that of a semiconductor with a large band gap. A new technique based or taking more than 100 readings for (V) and (I) is recommended to be used, to find the values of the energy gap. The magnetic properties of Gum Arabic show that it is a diamagnetic material. The refractive index is found to be in the range comparable with that of some previous studies Gum Arabic is an industrial material that could find

applications with the recent technologies. Therefore it is important to promote experimental techniques necessary to be and by use other types of Gums from different places [70].

3.5 Assessment of Physical Properties of Gum Arabic from Acacia Senegal Varieties in Baringo District, Kenya

The work done by J. K. Lelon was conducted to assess the physical properties of gum arabic obtained from two Acacia senegal varieties (var. Senegal and var.kerensis). In Marigat division, Baringo district. Gum Arabic samples from the experimental sites at Solit, Kapkun, Kimorok and Maoi were collected, dried and analysed to establish their physical characteristics. Moisture content in gum arabic obtained from variety kerensis in Kimorok and Maoi (17.5 ± 1.00 and 15.4 ± 0.50%) were significantly higher ($P < 0.05$) than those of variety senegal in Solit and Kapkun (15.0 ± 0.50 and 14.9 ± 1.80%), while internal energy(33.4 and 33.76%) were not significantly different ($P > 0.05$) from those of variety senegal found in Kapkun and Solit (33.0 and 32.96%), respectively. Ash content in gum Arabic from variety Senegal in Solit and Kapkun (2.94 and 3.16%) was higher ($P < 0.05$) than those of variety kerensis found in Kimorokand Maoi (2.88 and 2.72%). In Kapkun, volatile matter in gum arabic from variety Senegal (64.2%) is higher ($P < 0.05$) than the quantities of variety kerensis found in Kimorok, Solit and Maoi (63.8, 63.7 and63.6%), respectively. Moisture content in gum arabic from variety senegal in Solit and Kapkun (15.0 ±0.40 and 14.9 ± 1.80%) are within international specifications (13 to 15%), while variety kerensis in Kimorok and Maoi (17.5 and 15.4%) are does not obey the well known specifications. Moisture, ash and volatile matter contents in gum arabic from A. senegal variety senegal were 14.9, 3.16 and 64.24%, while A. Senegal variety kerens is had 15.2, 2.88 and 63.8%, respectively. Moisture, ash and volatile matter contents in gum arabic from A. Senegal variety senegal fell within international specifications while A. Senegal variety kerensis fell outside the specifications. Ash, volatile matter and internal energy contents in gum arabic from A. Senegal variety kerensis and variety Senegal are within the normal range. The gum arabic

from A. Senegal variety senegal in Solit and Kapkun was of better quality than that of A. senegal variety kerensis in Kimorok and Maoi [71].

3.6Gum Arabic-silver Nanoparticles Composite as A green Anticorrosive Formulation for Steel Corrosion in Strong Acid Media

In the work done by Moses M. Solomona a green anticorrosive composite (GA-AgNPs) has been formulated for steel in 15% HCl and 15% H_2SO_4 media. Characterization of GA-AgNPs is achieved using FTIR, UV-VIS, EDAX, and SEM. Gravimetric, electrochemical (EIS, EFM, DEIS, & TP), and surface assessment (SEM, EDAX, AFM, & XPS) techniques have been employed in the anticorrosion studies. Results from all applied methods potray GA-AgNPs as effective anticorrosive agent. Inhibition is by adsorption mechanism and follows Langmuir isotherm. GA-AgNPs acts as mixed type inhibitor in 15% H_2SO_4 solution but as anodic type in 15% HCl solution. Results from surface techniques confirm adsorption of GA-AgNPs molecules on specimen surface. Oxides, hydroxides, carbonates, and sulphates (H_2SO_4 medium) or chlorides (HCl medium) are the corrosion products in the free corrodent according to XPS results. In the presence of composite, both ionic and neutral forms of GA-AgNPS are adsorbed. AgNPs are present on the surface in the form: Ag, Ag_2O, and AgO. The conclusion of a green formulation consisting of gum Arabic, silver nanoparticles, and residual natural honey has been developed. The anticorrosion property of the prepared nanocomposite has been examined using several techniques. The results show that the composite is effective in inhibiting the steel corrosion in 15% $H_2SO_4$and 15% HCl solutions respectively. The composite molecules absorb onto the metal surface and protect the surface from further attack by aggressive agents present in the corrosive environments. The adsorption followed Langmuir adsorption isotherm model. GA-AgNPs acted as mixed type inhibitor in 15% H_2SO_4 solution but as anodic type inhibitor in 15% HCl solution. Inhibition is better in HCl medium. XPS results disclose that the corrosion products in the absent of composite are FeO,$FeCO_3$, Fe_2O_3, and

$FeSO_4$(H_2SO_4 medium) or FeCl3 (HCl medium). In the presence of composite, Gum Arabic is present in the adsorbed film inboth ionic and neutral forms while AgNPs are present in the form Ag, Ag_2O, and AgO[72].

3.7 Dopant profiling with the Scanning Electron Microscope - A study of Si

S. L. Elliott, R. F. Broom article describes semiconductor dopant profiling with the scanning electron microscope (SEM) using secondary electrons. We have demonstrated that contrast can be detected from p-doped regions as thin as one nanometer across. Contrast can also be measured from p-type regions with doping concentrations less than 10^{16} cm^{-3}. We have studied the variation of doping contrast with specimen temperature and with a bias applied across a p-n junction in situ in the SEM. These experiments demonstrate that doping contrast is mainly due to the built-in voltages in semiconductor devices which in local fields (patch fields) outside the specimen which influence the number of secondary electrons detected. The study show that c_{pn} varies linearly with the built-in voltage. The resolution and sensitivity limits of SEM dopant profiling have been systematically studied, with extremely promising results. Doped regions as small as one nanometer in width as well as dopant concentrations less than 10^{16} cm in p-type on n-type silicon have been detected. This article has provided experimental evidence linking dopant contrast to the built-in voltage at a semiconductor junction, by biasing a p-n junction and also by measuring the contrast over a range of temperatures. The results support the effect of local fields on the secondary electrons as the doped contrast mechanism. The results for a range of temperatures show a correlation between the built-in voltage and the magnitude of the doped contrast, in particular both the contrast (c_{pn}) and the built-in voltage (V_{bi}) decrease at higher tem-Broom, prelatures'. This result is particularly promising for the development of this technique, as quantification may be possible with further understanding of the contrast mechanism [73].

3.8 Classification and physicochemical characterization of Mesquite Gum (Prosopis spp.)

This research was made by Yolanda L. López-Franco .Under environmental stress conditions; mesquite trees can excrete a protein aceous arabinogalactan gum that is similar to Gum Arabic. The main physicochemical properties of the best-quality mesquite gum were determined and compared with those of gum Arabic. Additionally, the composition and molecular changes induced by purification processes were recorded. One batch (157 kg) of mesquite gum was categorized by subjective assessment into three classes (MGA, MGB and MGC) from high- to low-quality. Approximately 17.5% was classified as top-quality gum. It was found that this class of mesquite gum has lower humidity, inorganic and tannins content than the other classes, or even than the Gum Arabic sample used as a reference. All of the mesquite gum classes have higher protein content and lower intrinsic viscosity than gum Arabic. The purification processes were shown to reduce the content of lower molecular weight compounds that modify the interface properties of the gum. The results indicate that the proposed classification method can be used to select mesquite gum with physicochemical properties comparable to those of commercial gum Arabic. The conclusions was the proposed classification procedure is a simple method for the selection of mesquite gum that meets the quality requirements of the Joint FAO/WHO Expert Committee on Food Additives (JECFA) for gum Arabic intended for drugs and foods. The highest quality selected mesquite gum (MGA) has a lower tannin, insoluble solid, inorganic and humidity content than the other classes and even the gum Arabic used as a reference. Filtration and ultra filtration procedures can reduce the tannin content and the concentration of low molecular weight species in mesquite gum. However, these processes could modify the interface properties of the high quality mesquite gum (MGA)[74].

3.9 Electrical Conductivity Behavior of Gum Arabic Biopolymer-Fe_3O_4 Nanocomposites

The work done by D. Bhakat a study the electrical conduction properties of some composites of Gum Arabic biopolymer and magnetite nanoparticles as host and guest, respectively, synthesized in different weight percentages. The nanocomposites are found to be non-extrinsic type of semiconductors with guest content depend entrap distribution of charge carriers. Conductivity of these materials increases with increasing the impurities which is accompanied with decrease in the activation energy. Percolation theory has been employed for the analysis of the electrical conductivity results to explore the effect of the guest on the electrical conductivity of the host. Conductivity of these materials strongly depends temperature, applied bias voltage and the concentrations of the components. Increase of the impurities in the host material changes the nature of trap distribution in these nanocomposites. The activation energy of these samples is directly proportional to the concentration of the impurities. The small conductivity indicates that conduction takes place by the hopping in the presently studied samples, whereas in the non-Ohmic region the conduction may be controlled by quantum tunneling mechanism. Percolation concept has been applied to understand the electrical conduction in these composites. Percolation threshold and critical exponent are inversely proportional to the guest content. The conduction mechanism in these composites may be owing to the charge carrier transfer through the guest molecule aggregations distributed in the host matrix [75].

3.10 Determination of the Energy Gap of Gum Arabic Doped with Zinc Oxide Using the UV-VIS Technique

This work was by ELKHATEM ELMHDY ALI MOHAMED. In this work ,Zinc Oxide nano particle (ZnO) were successfully synthesized by asol-gel method, then the solution of the gum Arabic was also prepared and powered by the mortar method. The samples were characterized by UV-VIS spectroscopy technique. The energy gap of gum arabic is found to be, E_g =

(2.760) eV, for both samples. Which prove that it is a real semiconductor and its conductivity increases with the conductivity increasing. This shows that gum Arabic is semiconductor with conductivity increases upon increasing Zno concentration. [76].

3.11 Covalent Coupling of Gum Arabic onto Super Paramagnetic Iron Oxide Nanoparticles for MRI Cell Labeling: Physicochemical and in Vitro Characterization

This study has been done by Susana I. C. J . For this work Gum Arabic (GA) is a hydrophilic composite polysaccharide derived from exudates of Acacia senegal and Acacia seyal trees. It is biocompatible, possesses emulsifying and stabilizing properties and has been explored as coating agent of nanomaterials for biomedical applications, namely magnetic nanoparticles (MNPs). Previous studies focused on the adsorption of GA onto MNPs produced by co-precipitation methods. In this work, MNPs produced by a thermal decomposition method, known to produce uniform particles with better crystalline properties, were used for the covalent coupling of GA through its free amine groups, which increases the stability of the coating layer. The MNPs were produced by thermal decomposition of $Fe(acac)_3$ in organic solvent and, after lig and-exchange with meso-2,3-dimercaptosuccinic acid (DMSA), GA coating was achieved by the establishment of a covalent bond between DMSA and GA moieties. Clusters of several magnetic cores entrapped in a shell of GA were obtained, with good colloidal stability and promising magnetic relaxation properties (r_2/r_1 ratio of 350). HCT116 colorectal carcinoma cell line was used for in vitro cytotoxicity evaluation and cell-labeling efficiency studies. We show that, upon administration at the respective IC_{50}, GA coating enhances MNP cellular uptake by 19 times compared to particles bearing only DMSA moieties. Accordingly, in vitro MR images of cells incubated with increasing concentrations of GA-coated MNP present dose-dependent contrast enhancement. The obtained results suggest that the GA magnetic Nanosystem could be used as a MRI contrast agent for cell-labeling applications. GA was shown to contribute to high transverse and

low longitudinal MR relativity values (r_2/r_1 ratio of 350), resulting in good MRI contrast enhancement properties, observed both in phantom images of water dispersion of MNP-DMS-GA and in in vitro MRI images of HCT116 cells incubated with different concentrations of particles. By quantification of the cellular iron after incubation for 48 h with particles ,we showed that GA coating on MNP-DMSA enhances MNP cellular uptake by 19 times compared to MNP-DMSA alone. Incubation for different periods revealed that the iron uptake kinetics for MNP-DMSA-GA is fast (less than 12 h) and cellular uptake isalways enhanced compared to uncoated nanoparticles. After 48h of incubation, MNP-DMSA-GA localize in the lysosomes, which suggests uptake by endocytosis, but the evaluation of the presence of asialoglycoprotein receptors in the HCT116 cell line couldgive new insights on the MNP-DMSA-GA cellular uptake mechanism. We also found out that the HCT116 cell line is very sensitive to MNPs, given the observed dose-dependent cell viability decrease in MTT assay at the tested iron concentrations (IC_{50} values of 55 μg/mL for MNP-DMSA and 43 μg/mL for MNP-DMSA-GA).Apoptotic response was detected by up regulation of proapoptotic genes p21 and BAX and down regulation of anti apoptoticgene BCL-2 after 3.5 h and also at 48 h of incubation with the MNP-DMSA-GA nanoparticles (but to a lesser extent in this last time point). Nonetheless, given the large hydrodynamic diameter and the good MRI contrast enhancement properties, the MNP-DMSA-GA presents potential for in vitro MRI cell labeling applications. Further modification of GA (e.g., with a fluorophore or radionuclide) would contribute to a multimodal contrast agent, allowing to follow the labeled cells by MRI and other imaging technique(s) [77].

3.12Preparation, Characterization and Electrical Study of Gum Arabic /ZnO Nanocomposites

In the work done by PUSPENDU BARIK .Gum Arabic (GA)-mediated chemical synthesis was carried out for obtaining ZnO nanoparticles

(ZnONPs) (particle size of ZnO ≈ 40 nm) which, in turn, was used for preparing ZnO–biopolymer nanocomposites. The synthesized products were characterized by X-ray diffraction, Fourier transform infrared, and transmission electron microscopy for their structure and morphology. The frequency dependence of dielectric constant and dielectric loss of these GA–ZnO nanocomposites were analyzed in the frequency range of 100 Hz–5 kHz. In addition, the dielectric property of these nanocomposites (0–15 wt% filler concentration) was analyzed with respect to frequency in the temperature range 30–80◦C. A high dielectric constant of 275 is achieved for the sample with 10 wt% of ZnO filler. The dielectric property of GA–ZnO nanocomposites is attributed to the interfacial and orientation polarization. A high dielectric constant was found for the sample with 10 wt% of ZnO filler. The effect of ZnO on dielectric constant of nanocomposites was found to be more pronounced at lower frequency region. The dielectric properties of ZnO-NPs are attributed to the interfacial and orientation polarization. The synthesized composites exhibit a low dielectric loss at higher frequency region, which is preferred to reduce the energy dissipation and signal losses, particularly for high frequency applications [78].

CHAPTER FOUR

MATERIAL AND METHOD

4.1 Introduction:

This chapter contains the following, the materials, the method and instrumentation used in practical.

4.2 Materials

4.2.1 Gum Arabic

Two types of gum Arabic (Talha, Hashab) was used after processing.

4.2.2 Iodine (Iodine solution)

Iodine solution is iodine (I) and potassium iodide (KI) mixed with distilled water.

4.2.3Deionize Water

The processors are physically and water-free salts and the percentage of neutral acidity.

4.2.4Methanol (CH_3OH)

Methanol, also known as methyl alcohol. It is a light, volatile, colorless, flammable liquid with a distinctive alcoholic odor similar to that of ethanol

4.2.5 Sulfuric Acid (H_2SO_4)

Sulfuric acid, also known as oil of vitriol, is a mineral acid composed of the elements sulfur, oxygen and hydrogen. It is a colorless, odorless, and viscous liquid that is soluble in water and is synthesized in reactions that are highly exothermic.

4.3 Methods

Ten sample of Gum Arabic were doped by Iodine in different concentration were made by two group of material one was Talha Gum Arabic and the other Hashab Gum Arabic doping in five concentrations (0.1, 0.2, 0.3, 0.4 and 0.5)ppm. The preparing process started by preparing Hashab Gum Arabic solution by thermo chemical method where added 100 mL of methanol (Pour analysis 99%) with 50 mL (H_2SO_4) on the magnetic stiller were added to 5g of Hashab Gum Arabic .The resulting material was doped by Iodine in

different concentration in ice bath for 60 min to made five samples, using an intermediate test tube for the simple. And other doping five samples prepared by Talha Gum Arabic doping by Iodine in the same Hashab concentration. Then the annealed sample was grinded to get the powdered nanoparticles. The crystal structures of all samples were characterized at room temperature using a Philips PW1700 X-ray diffractometer (operated at 40 kV and current of 30 mA). The infrared spectra of synthesized FTIR (Fourier Transform Infrared Spectrophotometer) in the range of 400 to 4000 cm^{-1} which used to locate the band positions which are given for all samples. The optical properties of all samples were found at room temperature using min 1240 UV-Spectroscopy. From optical spectra of synthesized calculate all optical properties (Absorption Coefficient, Extinction coefficient, Optical Energy Band Gap, Refractive Index, Real Dielectric Constant and Imaginary Dielectric Constant)

4.5 Instrumental Analysis

4.5.1 X-Ray Diffraction (XRD)

X-ray diffractometers consist of three basic elements: an X-ray tube, a sample holder, and an X-ray detector. X-rays are generated in a cathode ray tube by heating a filament to produce electrons, accelerating the electrons toward a target by applying a voltage, and bombarding the target material with electrons. When electrons have sufficient energy to dislodge inner shell electrons of the target material, characteristic X-ray spectra are produced. These spectra consist of several components, the most common being K_α and K_β. K_α consists, in part, of $K_{\alpha1}$ and $K_{\alpha2}$. $K_{\alpha1}$ has a slightly shorter wavelength and twice the intensity as $K_{\alpha2}$. The specific wavelengths are characteristic of the target material (Cu, Fe, Mo, and Cr). Filtering, by foils or crystal monochrometers, is required to produce monochromatic X-rays needed .for diffraction. Kα1and Kα2 are sufficiently close in wavelength such that a weighted average of the two is used. Copper is the most common target material for single-crystal diffraction, with Cu K_α radiation = 1.5418Å. These

X-rays are collimated and directed onto the sample. As the sample and detector are rotated, the intensity of the reflected X-rays is recorded. When the geometry of the incident X-rays impinging the sample satisfies the Bragg Equation, constructive interference occurs and a peak in intensity occurs. A detector records and processes this X-ray signal and converts the signal to a count rate which is then output to a device such as a printer or computer monitor.

The geometry of an X-ray diffractometer is such that the sample rotates in the path of the collimated X-ray beam at an angle θ while the X-ray detector is mounted on an arm to collect the diffracted X-rays and rotates at an angle of 2θ. The instrument used to maintain the angle and rotate the sample is termed a goniometer. For typical powder patterns, data is collected at 2θ from ~5° to 70°, angles that are preset in the X-ray scan. [79]

Figure (4.1) X-Ray diffract meter: XRD (wavelength 1.54 A°).

4.5.2 Ultraviolet–Visible Spectroscopy

The visible spectra obtained in shimadzo mini 1240 spectrophotometer scanning between 200 -1200 nm. The spectrophotometer measures how much of the light is absorbed by the sample .the intensity of light before e going into a certain sample is symbolized by Io. The intensity of light remaining after it had gone through the sample is symbolized by I. the fraction of light

transmitted is (I_o/I) which is usually expressed as percent transmittance (%T)from this information ,the absorbance of the sample is determined for that wavelength or as function for ranger of wavelength .sophisticated UV/VIS spectrophotometers often do this automatically. Although the sample could be solid (or even gaseous, they are usually liquid).A transparent cell, often called cavetti. It used to hold a liquid sample in spectrophotometer. The path length L through the sample is then the width of the cell through which the light passes through. Simple (economic) spectrophotometer may use cavetti shape like cylindrical test tubes, but more sophisticated one use rectangular cavity common 1cm in width for just visible 46 spectroscopy, ordinary glass cavity may be used, but ultraviolet spectroscopy requires special cavities made of UV transparent materials such as quartz. An ultraviolet visible spectrum is essentially a graph of light absorbance vs. Wave length in arrange of ultraviolet or visible regions[26].

Figure (4.2) Ultraviolet–Visible Spectroscopy.

4.5.3 Fourier Transform Infrared Spectroscopy (FTIR)

Fourier transform infrared (FTIR) spectroscopy is one of the most powerful tools for the determination of functional group in a membrane together with possible molecular bonds between chemical compounds of membrane. Fourier transform spectrophotometer provides the IR spectrum much more rapidly compared to the traditional spectrophotometer. Fig. 4.3 schematically illustrates the main component of a simple FTIR spectrophotometer. The

instrument produces a beam of IR irradiation, which is emitted from a glowing black-body source. Subsequently, the beam passes through into interferometer where the spectral encoding takes place. The recombination of beams with different in path lengths in the interferometer creates constructive and destructive interference called an interferogram. The beam now enters the samples compartment and the sample absorbs specific frequencies of energy, which are uniquely characteristic of the sample from the interferogram. Then, the detector measures the special interferogram signal in energy versus time for all frequencies simultaneously. In the meantime, a beam is superimposed to provide a reference (background) for the instrument operation. Finally, the desirable spectrum was obtained after the interferogram automatically subtracted the spectrum of the background from the sample spectrum by Fourier transformation computer software [80].

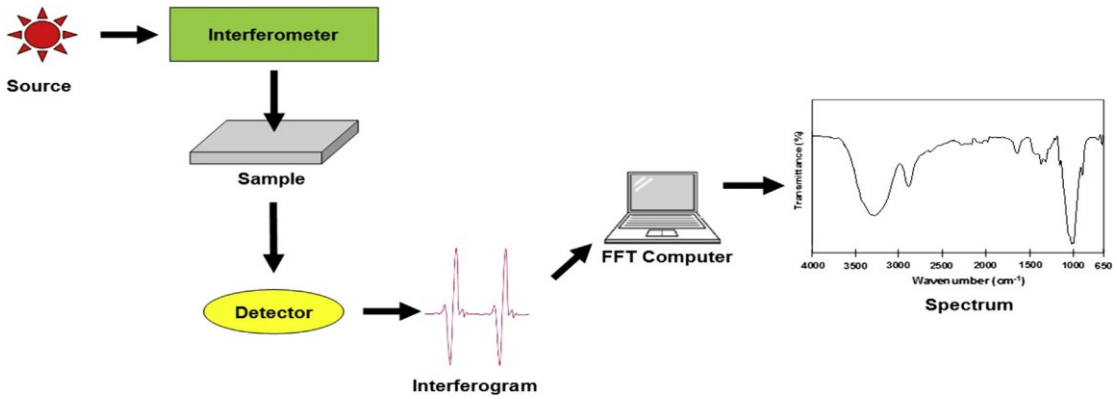

Figure (4.3) Basic Component in Fourier Transform Infrared Spectrometer.

Figure (4.4) FTIR Spectroscopy, Satellite Serial No 20010102.

4.5.4 Scanning Electronic Microscope (SEM)

A scanning electron microscope (SEM) is the technique of choice for analysis of specimen surfaces [81, 82]; provide information on surface topography, crystalline structure, chemical composition and electrical behaviour of the top 1 μm or so of specimen [83]. It is a type of electron microscope that produces images of a sample by scanning the surface with a focused beam of electrons. The electrons interact with atoms in the sample, producing various signals that contain information about the sample's surface topography and composition. The electron beam is scanned in a raster scan pattern, and the beam's position is combined with the detected signal to produce an image. SEM can achieve resolution better than 1 nanometer. Specimens can be observed in high vacuum in conventional SEM, or in low vacuum or wet conditions in variable pressure or environmental SEM, and at a wide range of cryogenic or elevated temperatures with specialized instruments. [84]The most common SEM mode is detection of secondary electrons emitted by atoms excited by the electron beam. The number of secondary electrons that can be detected depends, among other things, on specimen topography. By scanning the sample and collecting the secondary electrons that are emitted using a special detector, an image displaying the topography of the surface is created.

Figure (4.5) Scanning Electronic Microscope SEM device manufactured by Shimadzu company–Japan.

CHAPTER FIVE
RESULTS, DISCUSSION, CONCLUSSION AND RECOMMENDATION

5.1 Introduction

In this chapter we will deal with the practical experiments that were done, and the results obtained in addition to the amount of these results,

5.2 Results

5.2.1 Gum Arabic Doping by Iodine XRD Results

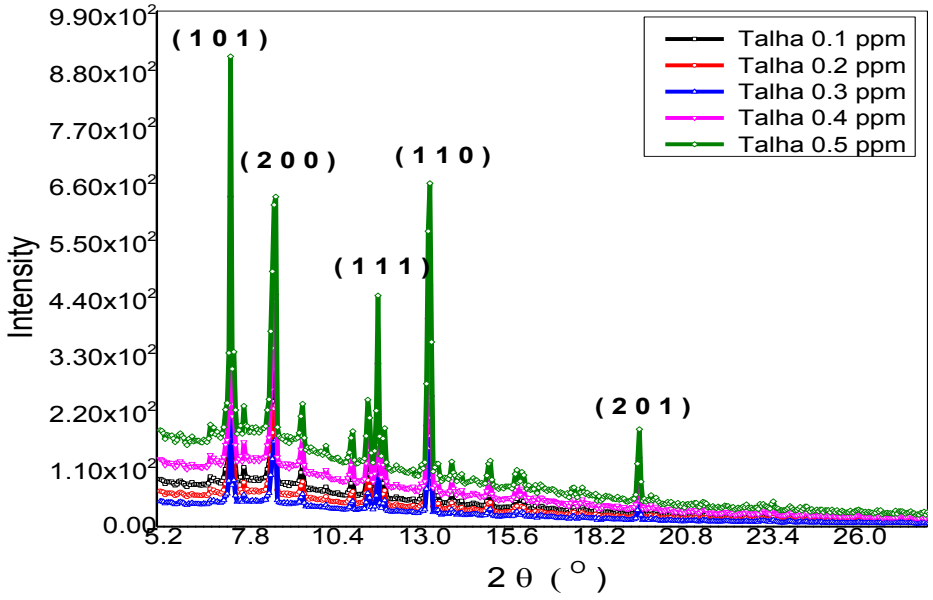

Figure (5.1) the XRD charts of the five samples Talha Gum Arabic doped by iodine (0.1 ,0.2,0.3,0.4 and 0.5) ppm

The crystal structure of all samples was characterized at room temperature using a Philips PW1700 X-ray diffract meter (operated at 40 kV and current of 30 mA) and samples were scanned between 6° and 27° at a scanning speed of 0.06 °C/s using Cu K_α radiation with $\lambda = 1.5418$Å. The X-ray diffraction patterns of the synthesized Talha Gum Arabic doped by iodine (0.1 ,0.2,0.3,0.4 and 0.5) ppm have been shown in Fig (5.1). The existence of the (101), (200), (111), (110) and (201) major lattice planes in the XRD patterns

confirms the formation of spinel (Cubic /Primitive for 0.1 ppm , Monoclinic/C-Center for 0.2 ppm, Hexagonal/Primitive for 0.3 ppm , Monoclinic/C-Center for 0.4 ppm and Triclinic/Primitive for 0.5 ppm), Miller indices provided in the figure and all peaks determine transformation of dried Talha gum doped by iodine.

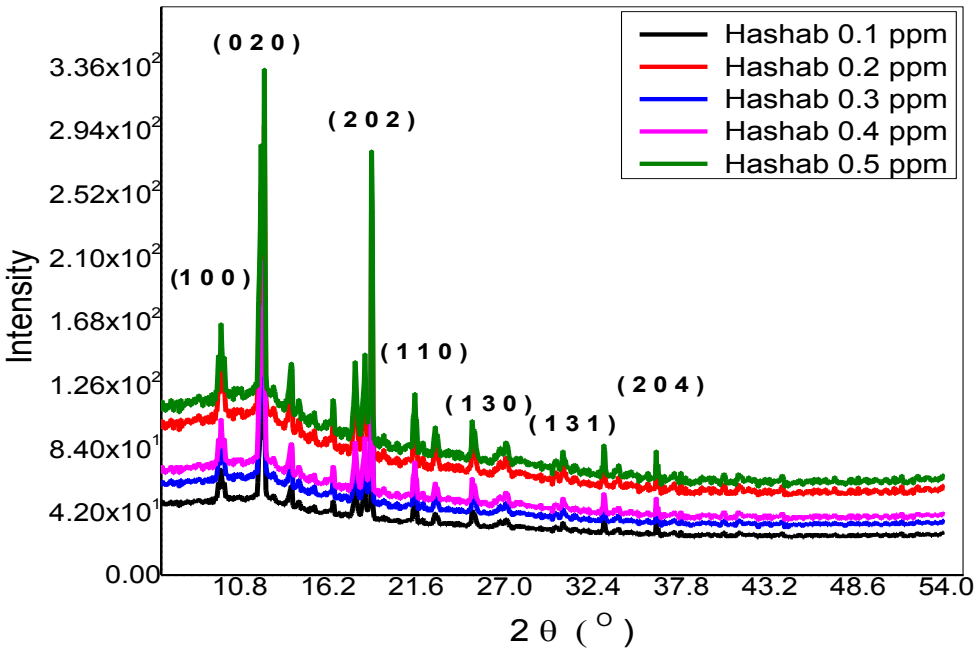

Figure (5.2) The XRD charts of the five samples Hashab Gum Arabic doped by iodine concentrations(0.1 ,0.2,0.3,0.4 and 0.5 ppm)

The X-ray diffraction patterns of the synthesized of Hashab Gum Arabic doped by iodine (0.1 ,0.2,0.3,0.4 and 0.5) ppm have been shown in Fig (5.2). The existence of the (100), (020), (202), (110) ,(130) ,(131) and (204) major lattice planes in the XRD patterns confirms the formation of spinel (Orthorhombic/C-Center for 0.1 ppm , Orthorhombic/Primitive for 0.2 ppm, Cubic /F-Center for 0.3 ppm , Hexagonal/Primitive for 0.4 ppm and Tetragonal/I-Center for 0.5 ppm), Miller indices provided in the figure and all peaks determine transformation of dried Hashab gum doped by iodine.

Table (5.1) Some crystallite lattice parameter (c- form , a,b,c, β,α, γ, density ,Xs(nm) and d – spacing) of all samples that meade by Gum Arbic (Talha and Hashab)

Sample	C-form	A	B	C	A	β	γ	Density	Xs(nm)	d-spacing
Talha 0.1 ppm	Cubic /Primitive	14.166	14.166	14.166	90	90	90	1.6838	91.62	8.13
Talha 0.2 ppm	Monoclinic/C-Center	16.575	3.155	6.231	90	90	90	2.029	83.14	7.58
Talha 0.3 ppm	Hexagonal/Primitive	13.887	13.887	40.988	90	90	120	3.4979	76.25	7.13
Talha a 0.4 ppm	Monoclinic/C-Center	10.467	4.855	8.281	90	109	90	4.1179	63.27	6.53
Talha 0.5 ppm	Triclinic/Primitive	7.228	7.829	7.945	105	96	92.9	4.937	55.51	6.21
Hashab 0.1 ppm	Orthorhombic/C-Center	20.622	9.724	19.623	90	90	90	1.6227	89.25	9.12
Hashab 0.2ppm	Orthorhombic/Primitive	13.62	14.4	12.6	90	90	90	1.7425	71.35	8.36
Hashab 0.3 ppm	Cubic /F-Center	3.5667	3.5667	3.5667	90	90	90	3.5145	66.81	7.82
Hashab 0.4 ppm	Hexagonal/Primitive	8.948	8.948	14.078	90	90	90	3.555	58.22	6.22
Hashab 0.5 ppm	Tetragonal/I-Center	6.3974	6.3974	9.2561	90	90	90	4.4261	51.24	5.89

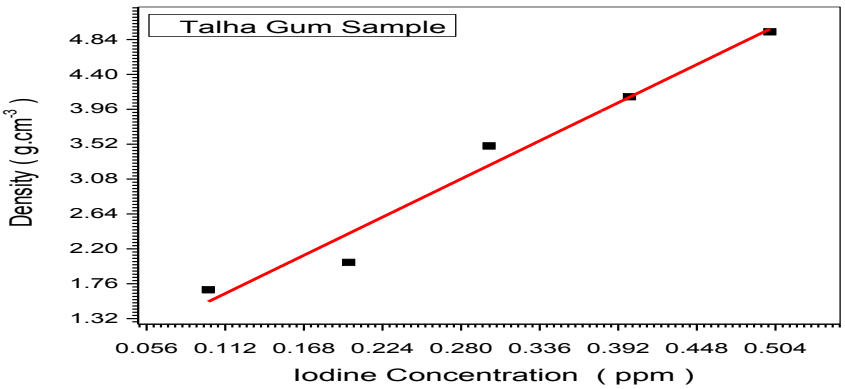

Figure (5.3) Dependence of the density of Talha Gum Arabic samples on iodine concentration

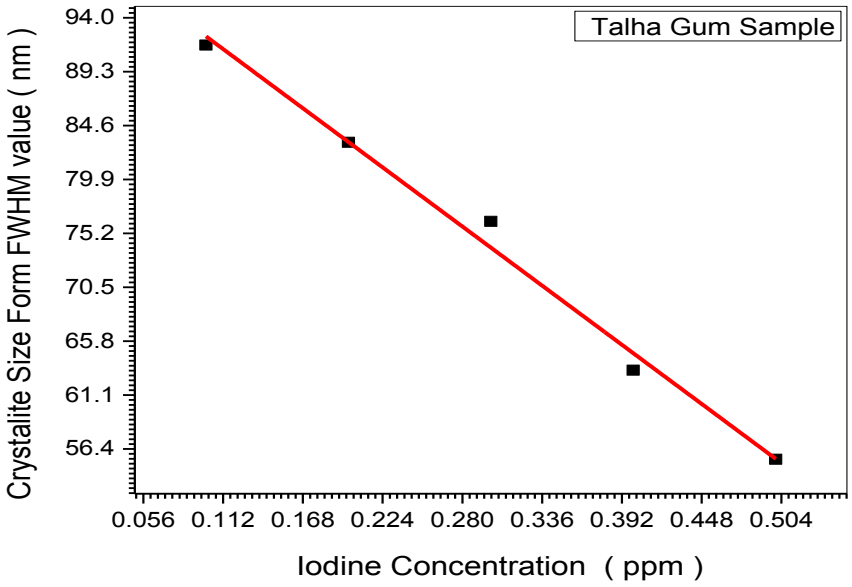

Figuer (5.4)Dependence of the crystallites growth of Talha Gum Arabic samples on iodine concentration

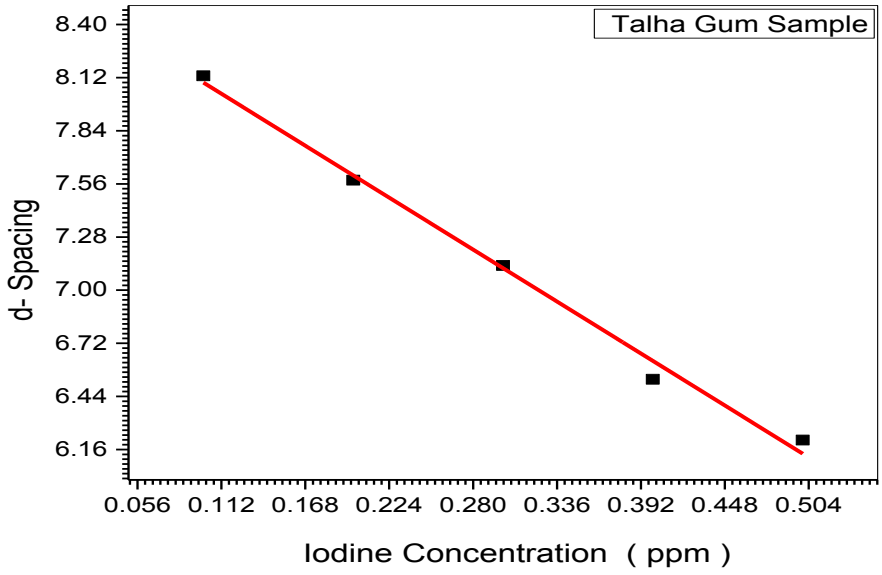

Figure(5.5)Dependence of the d- spacing of Talha Gum Arabic samples on iodine concentration

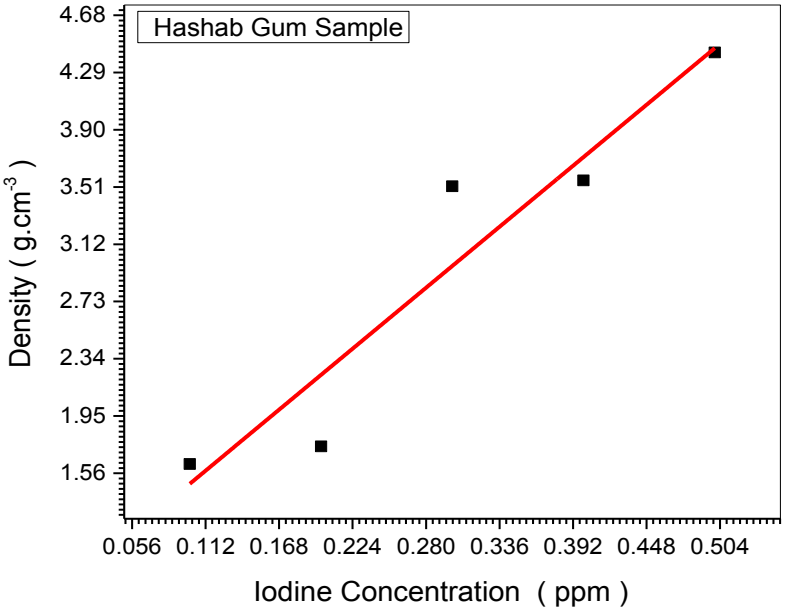

Figure (5.6)Dependence of the density of the Hashab Gum Arabic samples on iodine concentration

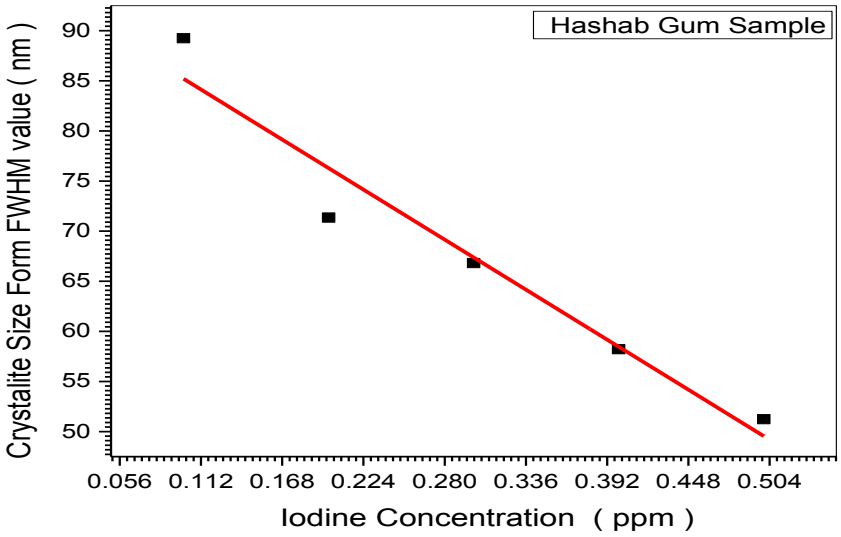

Fig(5.7) Dependence of the crystallites growth of the Hashab Gum Arabic samples on iodine concentration

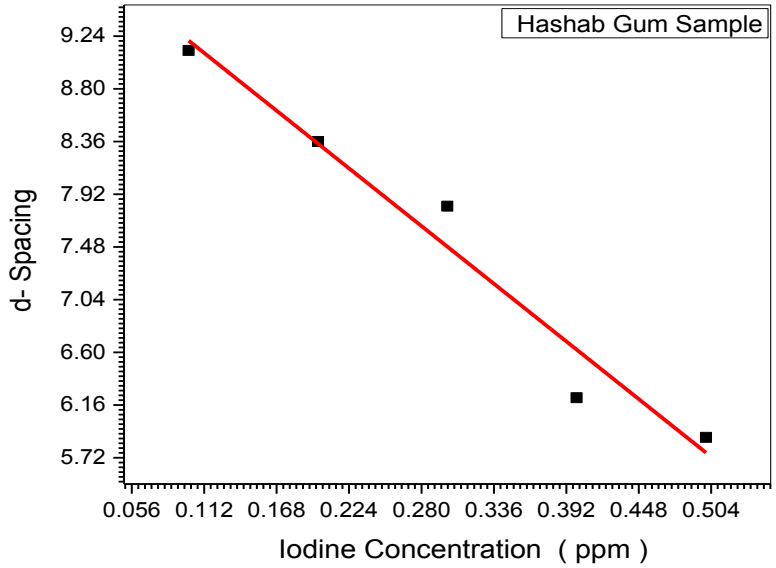

Figure(5.8)Dependence of the d- spacing of the Hashab Gum Arabic samples

5.2.2 Talha Gum Optical Properties Results

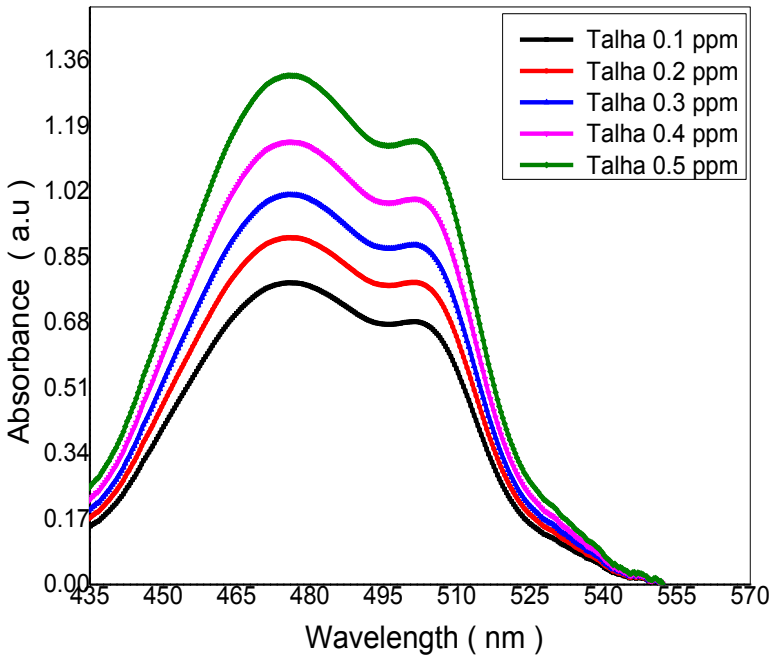

Figure(5.9) plots the relation of wavelengths vrs absorbance of Talha Gum Arabic doped by iodine having different concentrations

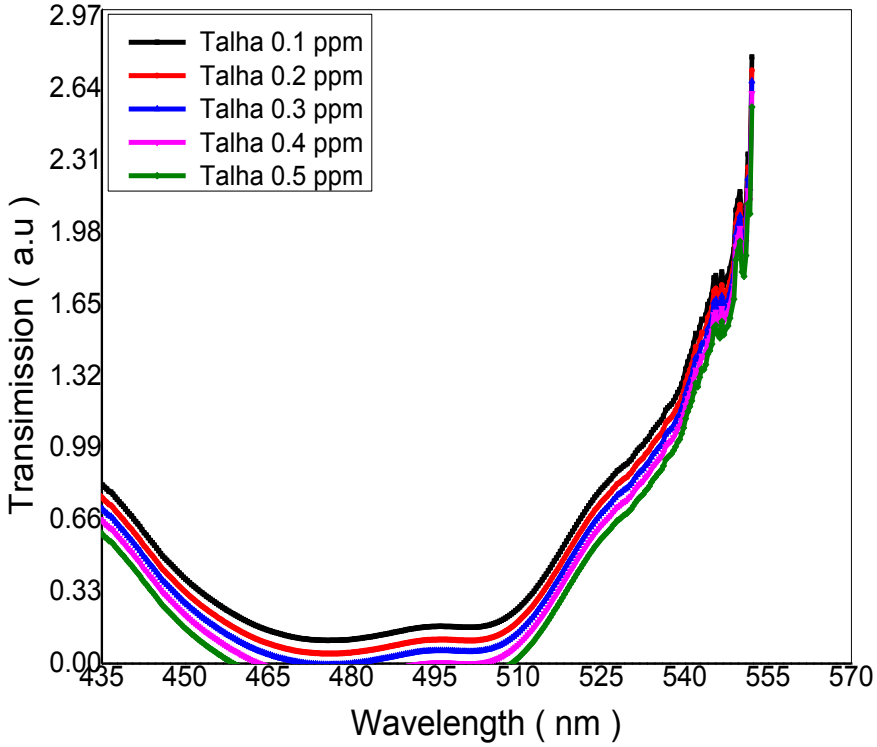

Figure(5.10) plots the relation between transmission and wavelengths of five sample that made by Talha Gum doped by iodine having different concentrations

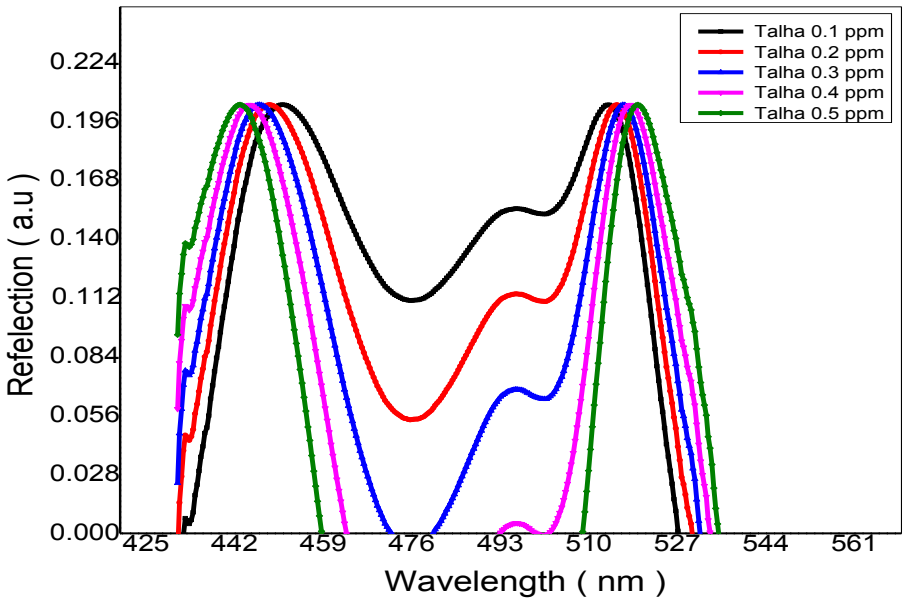

Figure(5.11) plots the relation of wavelengths vrs reflection of Talha Gum Arabic doped by iodine having in different concentrations

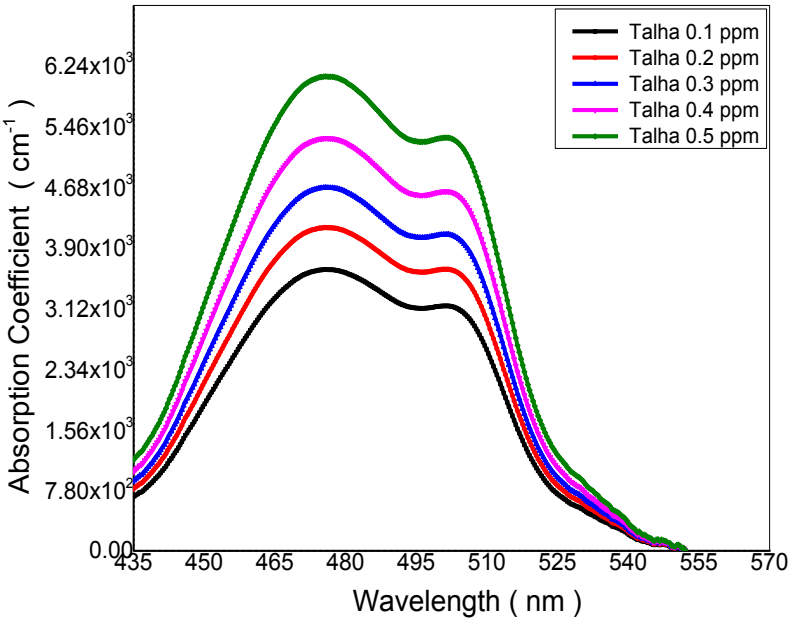

Figure(5.12) plots the relation of wavelengths vrs absorption coefficient of Talha Gum Arabic doped by iodine in different concentrations

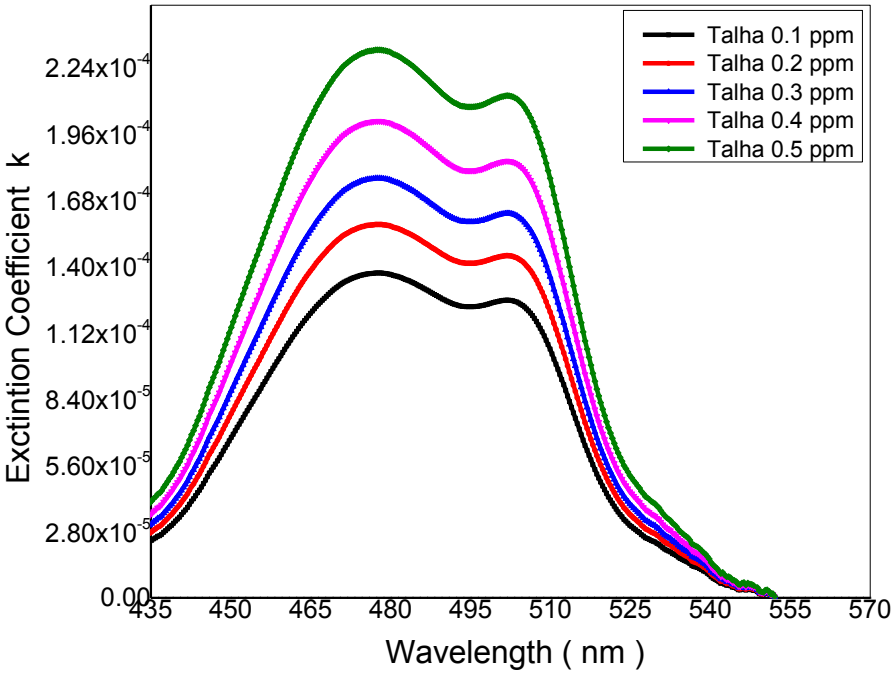

Figure(5.13) plots the relation of wavelengths vrs exctintion coefficient of Talha Gum Arabic doped by iodine in different concentrations

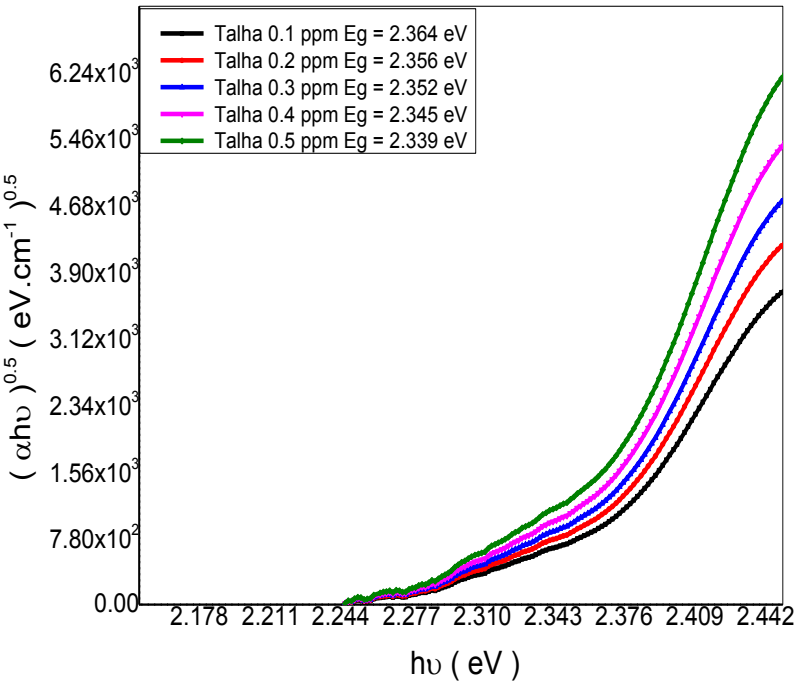

Figure(5.14) plots the optical energy band gap of Talha Gum doping by iodine in different concentrations

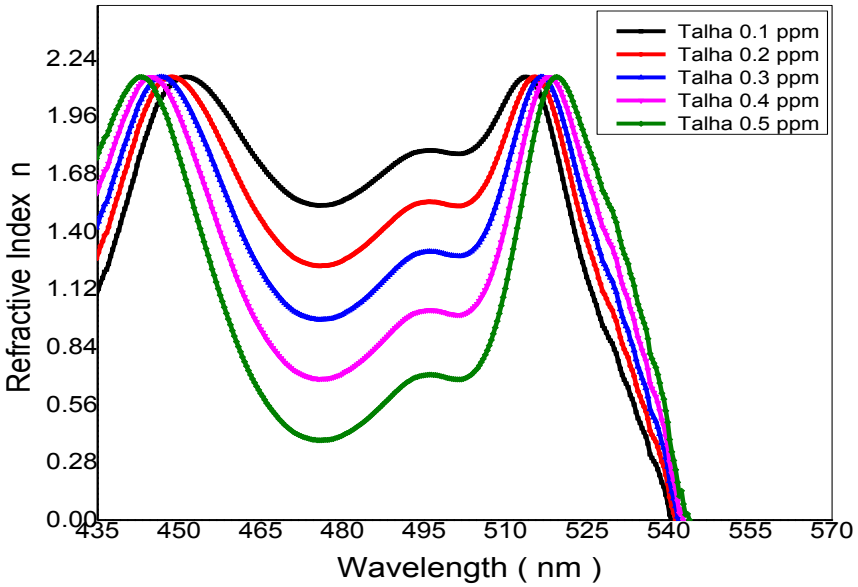

Fig(5.15) plots the relation of wavelengths vrs refractive index of Talha Gum Arabic doped by iodine in different concentrations

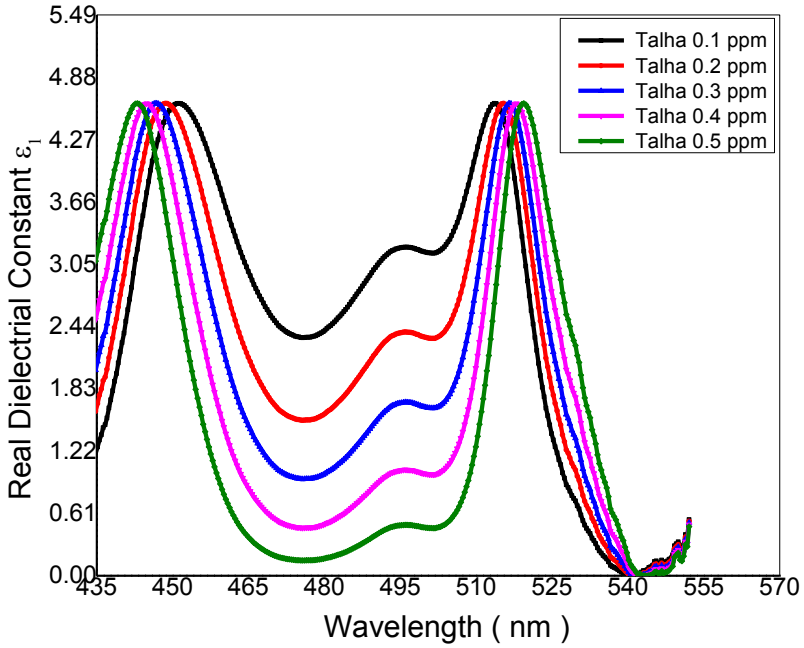

Figure(5.16) plots the relation of wavelengths vrs real dielectric constant of Talha Gum Arabic doped by iodine in different concentration

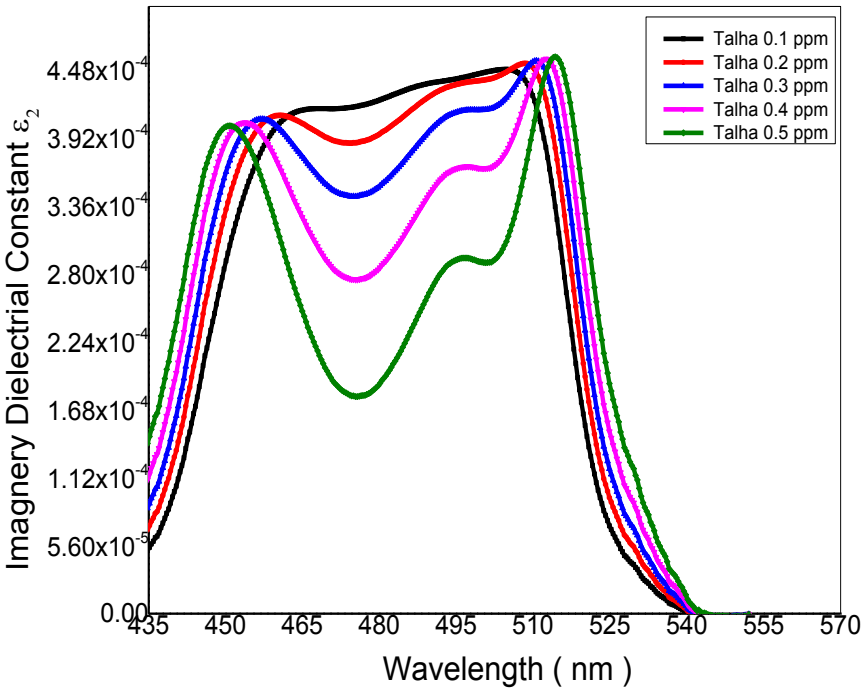

Figure(5.17) plots the relation of wavelengths vrs imaginary dielectric constant of Talha Gum Arabic doped by iodine in different concentrations

5.2.3 Hashab Gum Optical Results

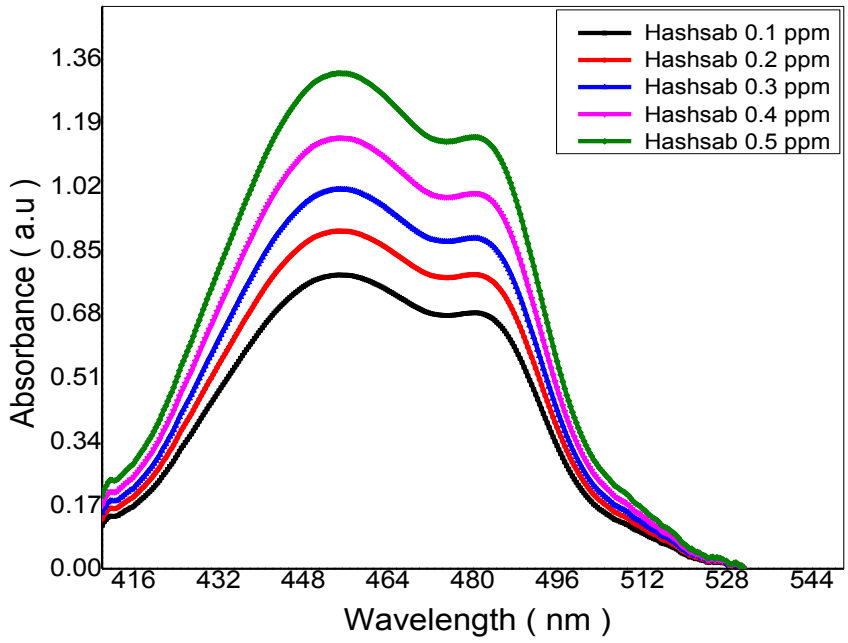

Fig(5.18) plots the relation of wavelengths vrs absorbance of Hashab Gum Arabic doped by iodine in different concentrations

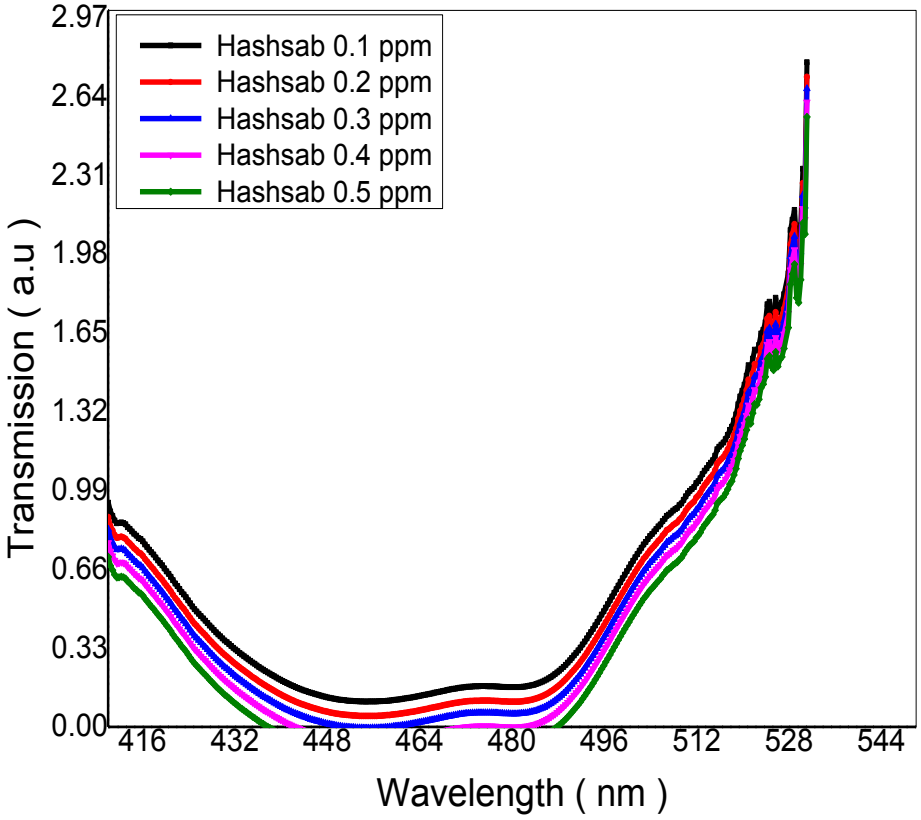

Figure(5.19) plots the relation of wavelengths vrs transmission of Hashab Gum Arabic doped by iodine in different concentrations

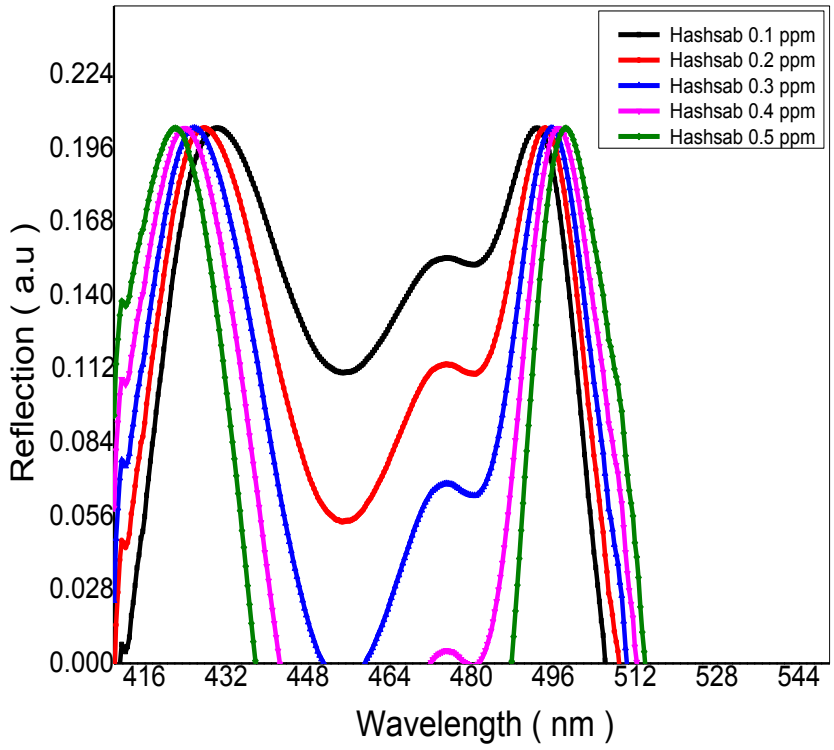

Figure(5.20) plots the relation of wavelengths vrs reflection of Hashab Gum Arabic doped by iodine in different **concentrations**

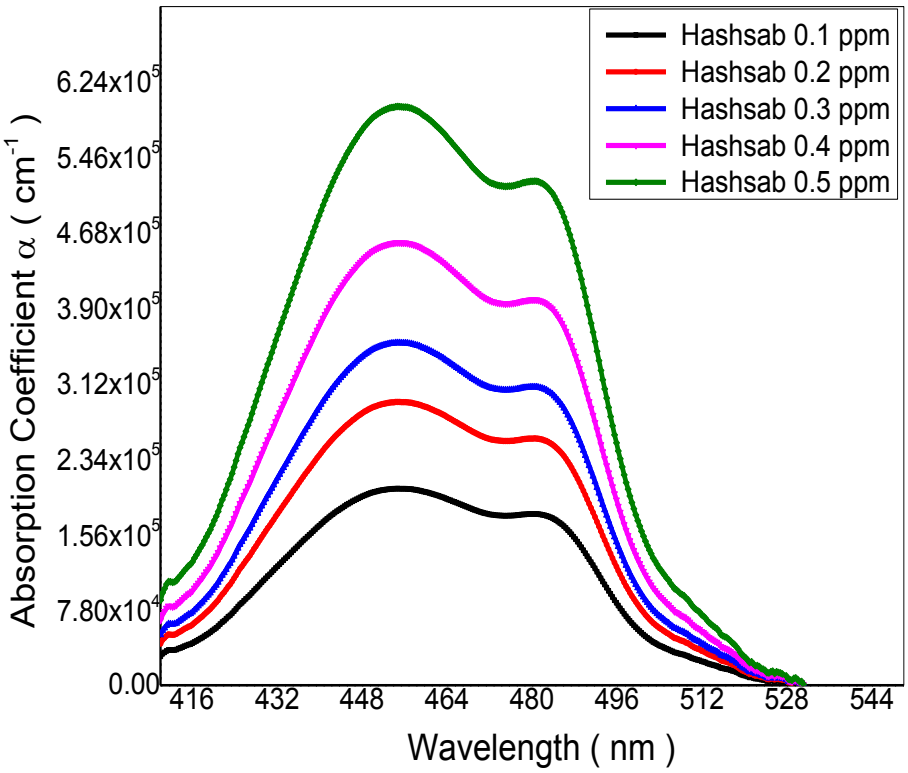

Figure(5.21) plots the relation of wavelengths vrs absorption coefficient of Hashab Gum Arabic doped by iodine in different concentrations

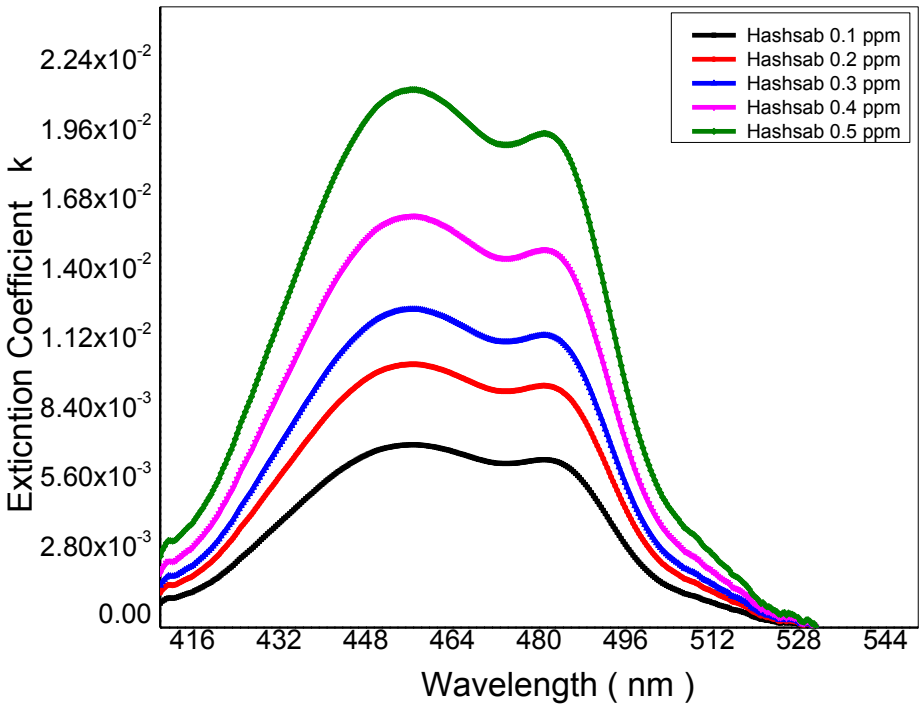

Figure(5.22) plots the relation of wavelengths vrs exctintion coefficient of Hashab Gum Arabic doped by iodine in different concentrations

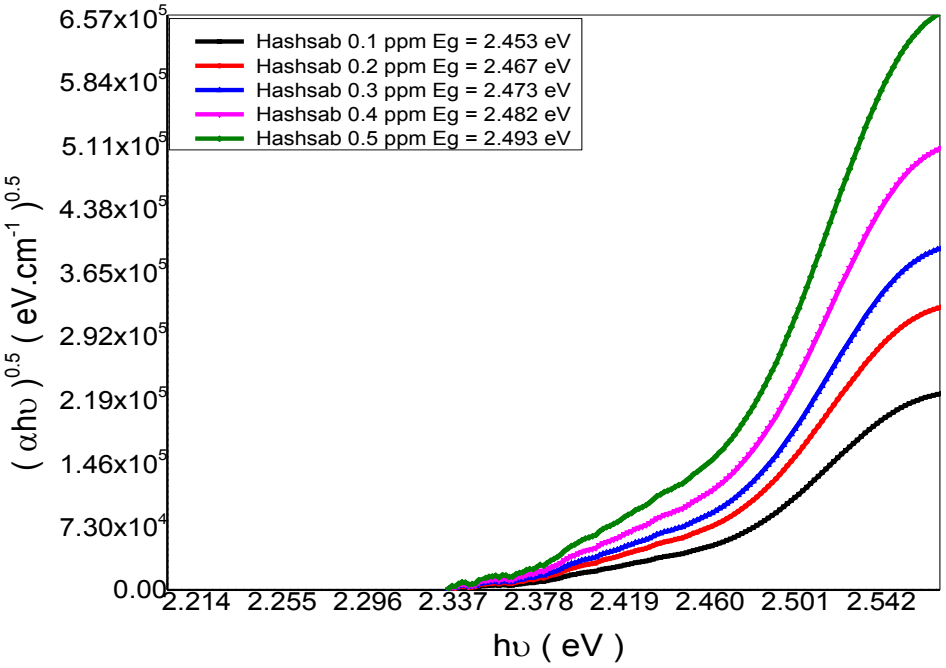

Figure(5.23) optical energy band gap of five sample that made by Hashab Gum Arabic doped by iodine in different concentrations

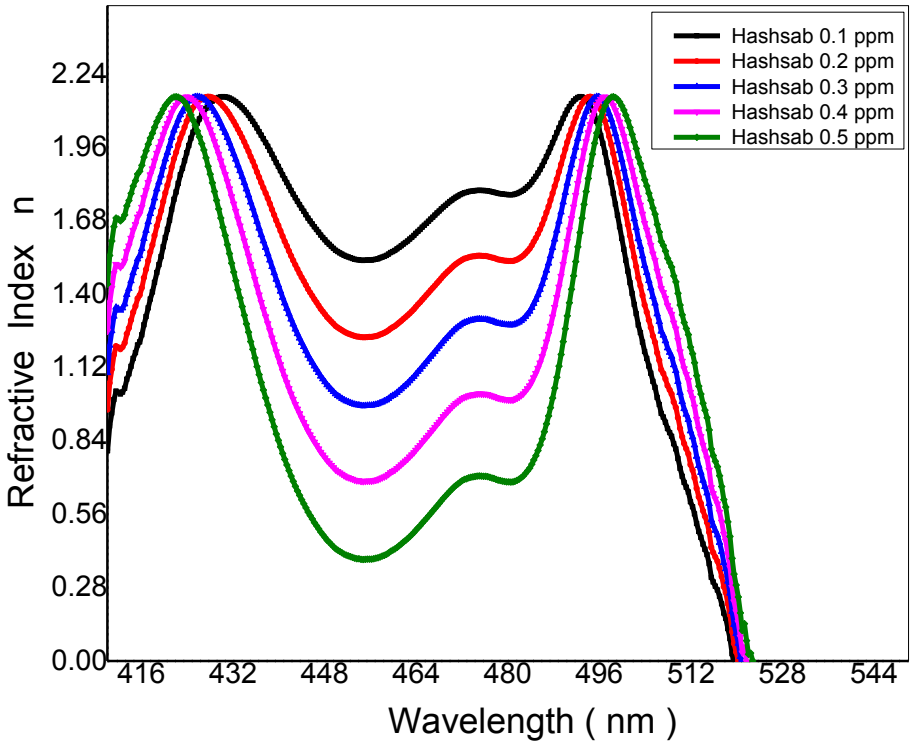

Fig(5.24) plots the relation of wavelengths vrs refractive index of Hashab Gum Arabic doped by iodine in different concentrations

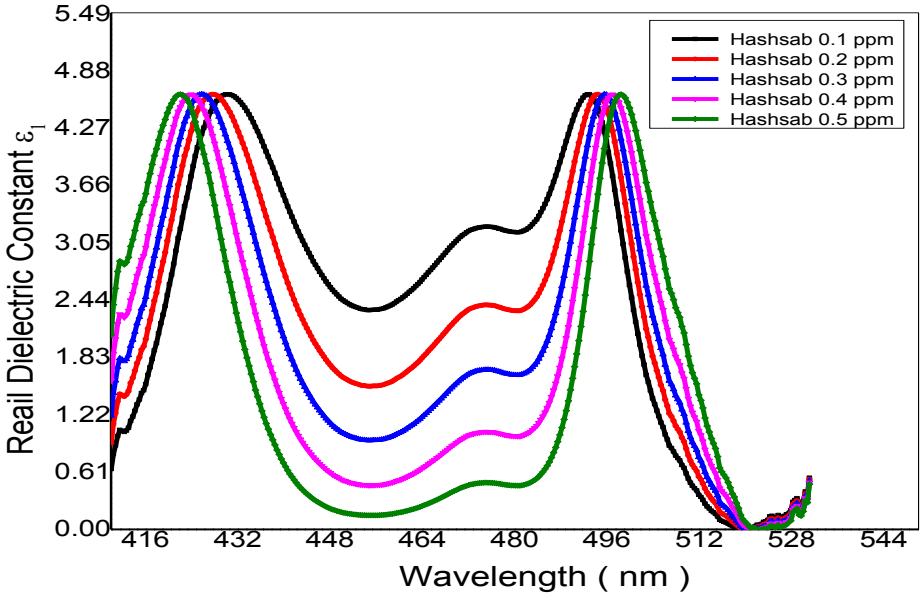

Figure(5.25) plots the relation of wavelengths vrs real dielectric constant of Hashab Gum Arabic doped by iodine in different concentrations

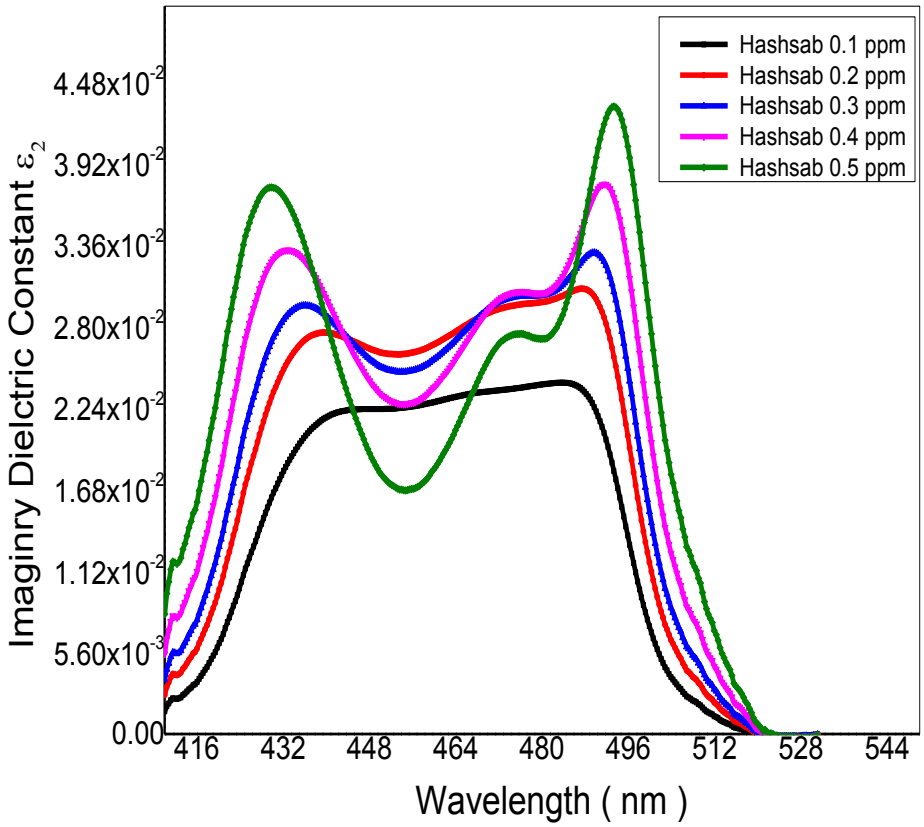

Figure(5.26) plots the relation of wavelengths vrs imaginary dielectric constant of Hashab Gum Arabic doped by iodine in different concentrations

5.2.4 SEM Talha Gum Arabic Results

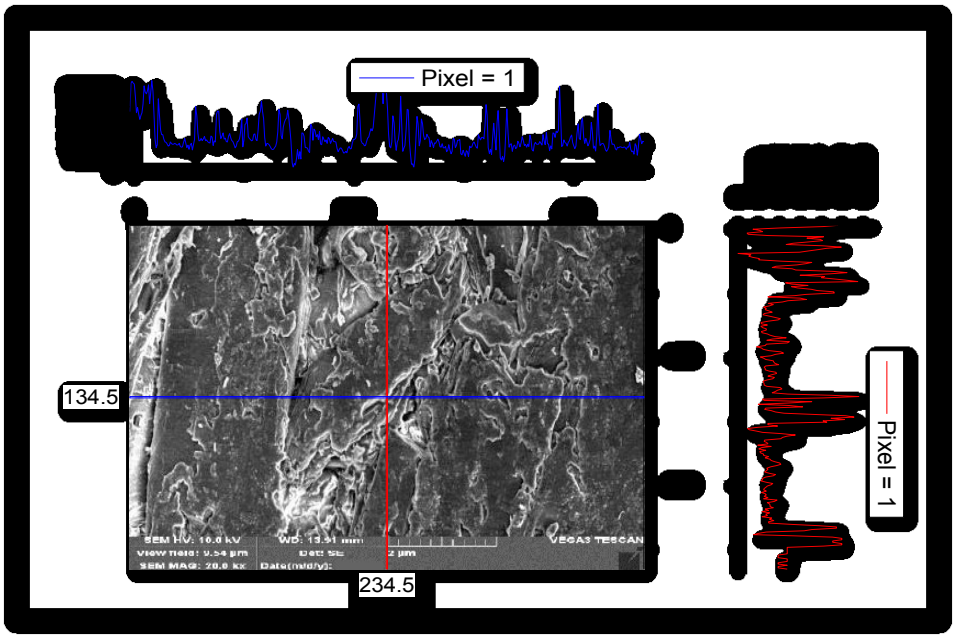

Figure (5.27) SEM images of the Talha Gum Arabic having 0.1 ppm concentration

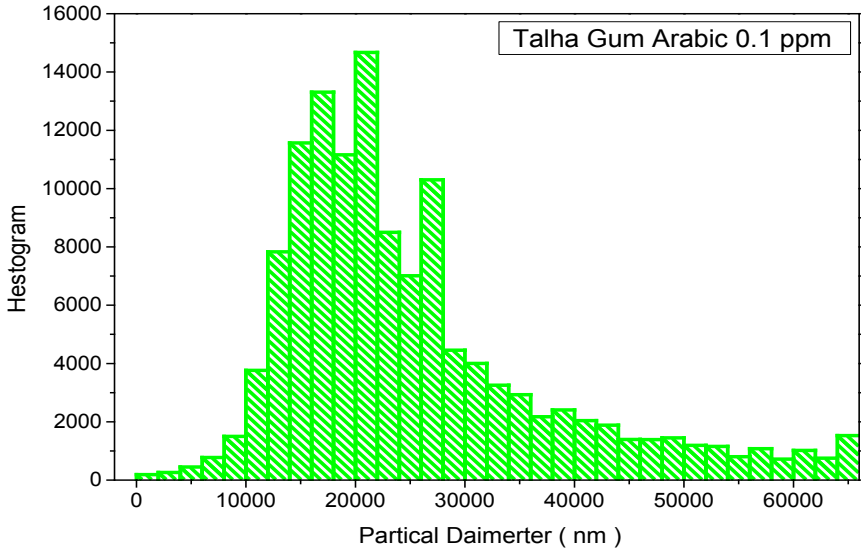

Figure (5.28) Particle diameter distribution of Talha Gum Arabic having 0.1 ppm concentration

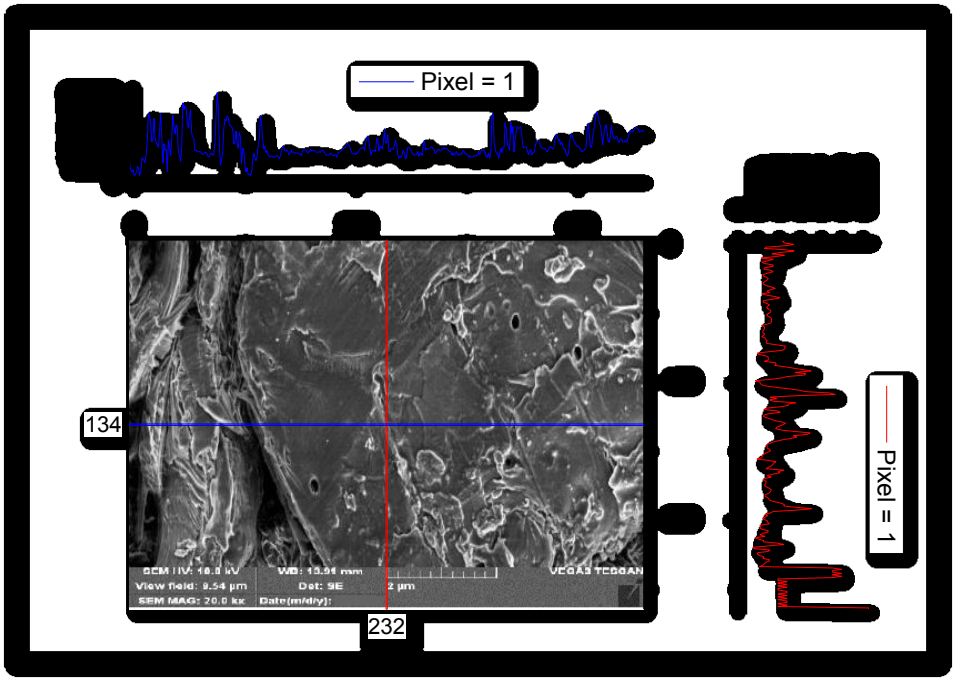

Figure (5.29) SEM images of the Talha Gum Arabic having 0.2 ppm concentration

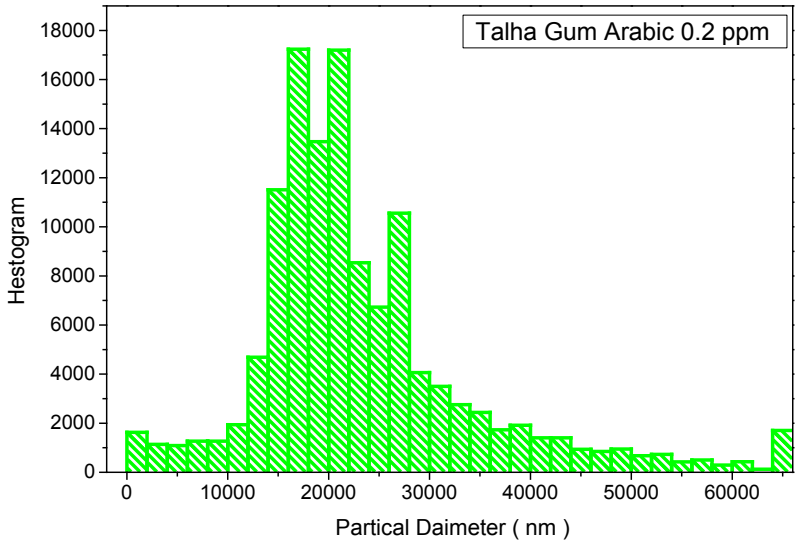

Figure (5.30) Particle diameter distribution of Talha Gum Arabic having 0.2 ppm concentration

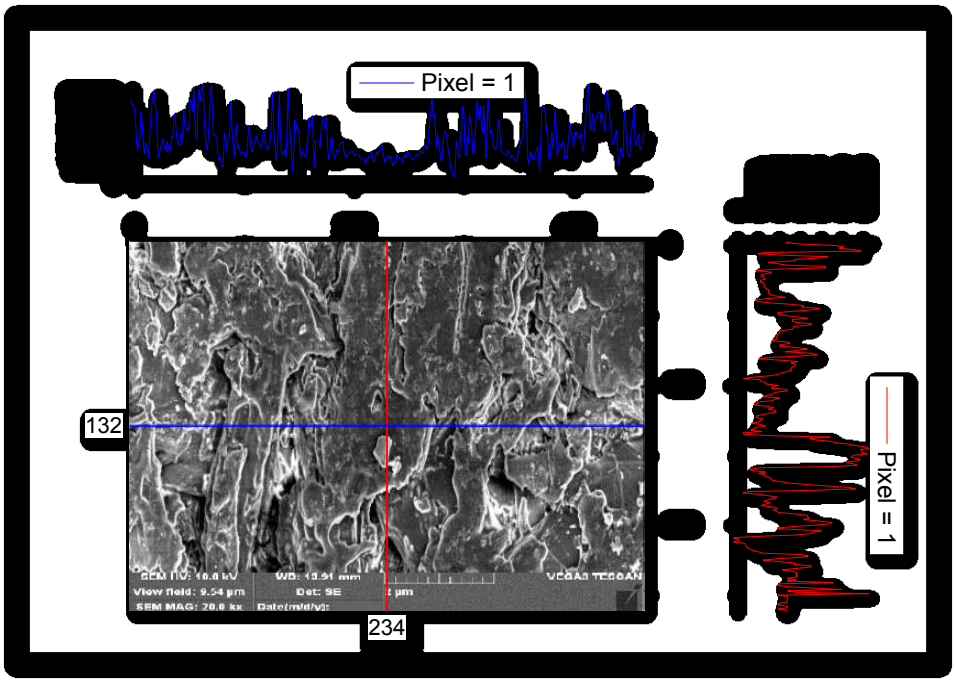

Figure (5.31) SEM images of the Talha Gum Arabic having 0.3 ppm concentration

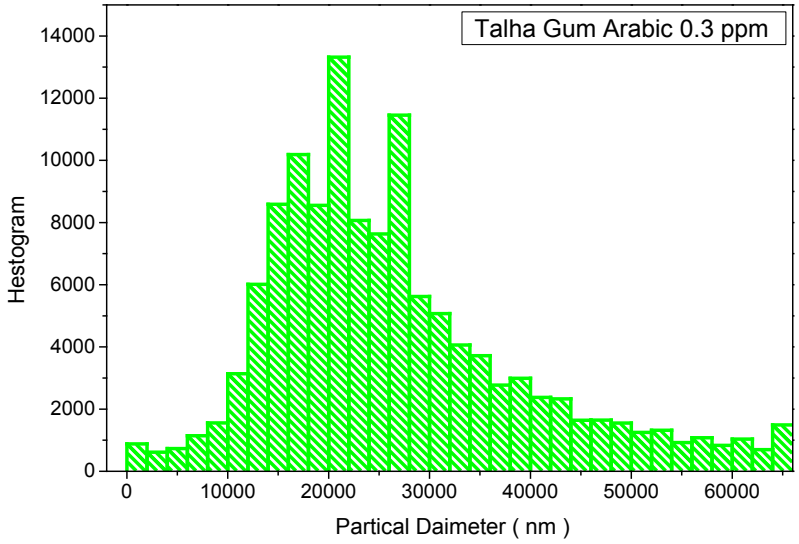

Figure (5.32) Particle diameter distribution of Talha Gum Arabic having 0.3 ppm concentration

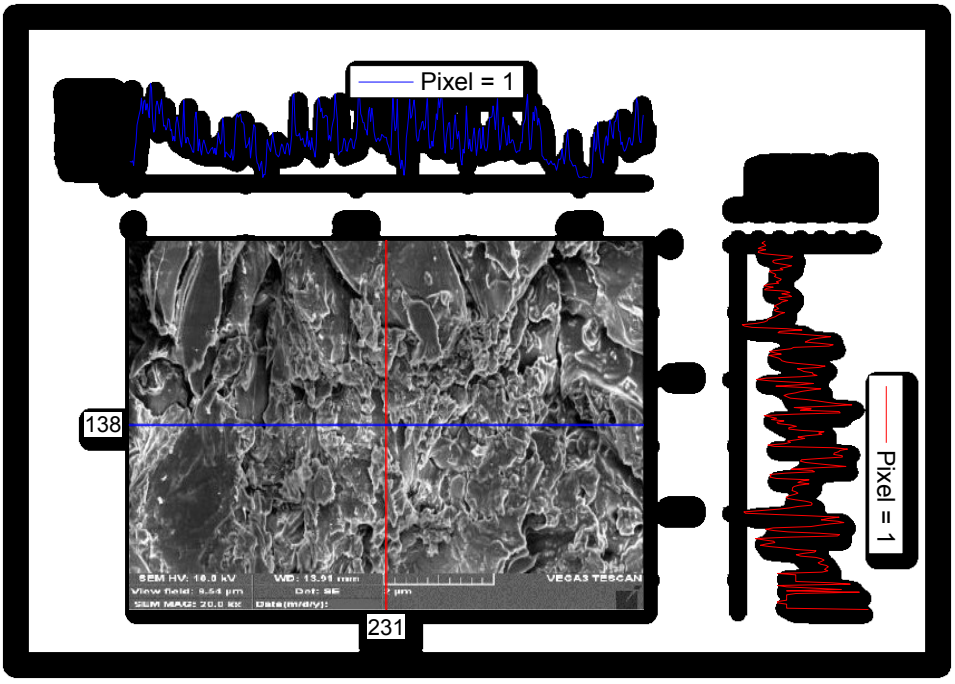

Figure (5.33) SEM images of the Talha Gum Arabic having 0.4 ppm concentration

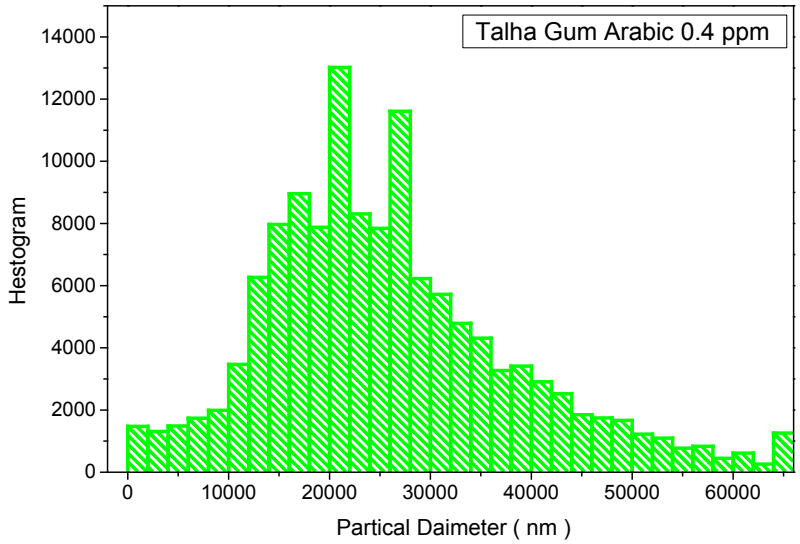

Figure (5.34) Particle diameter distribution of Talha Gum Arabic having 0.4 ppm concentration

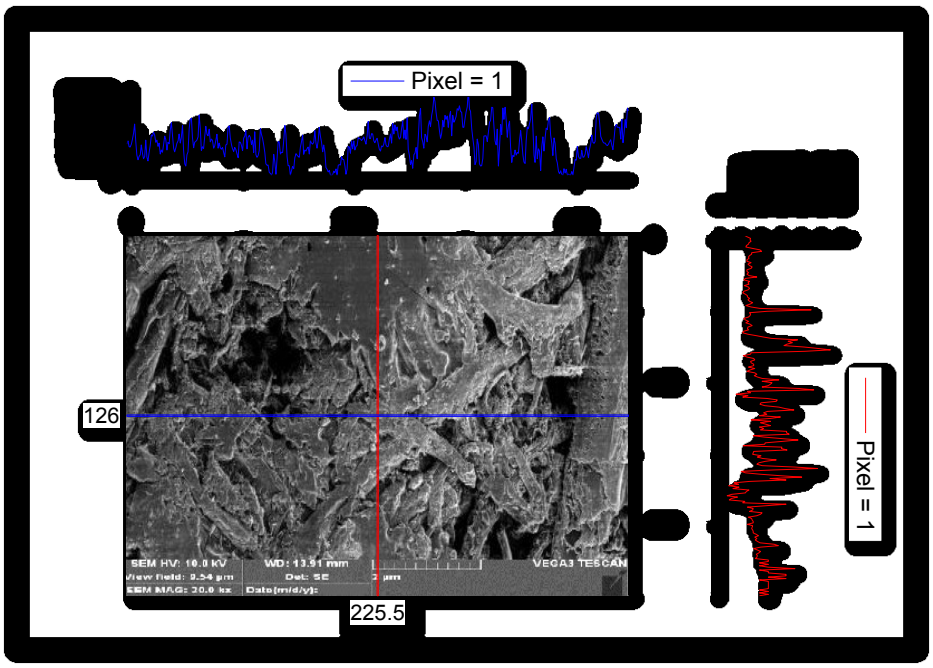

Figure (5.35) SEM images of the Talha Gum Arabic having 0.5 ppm concentration

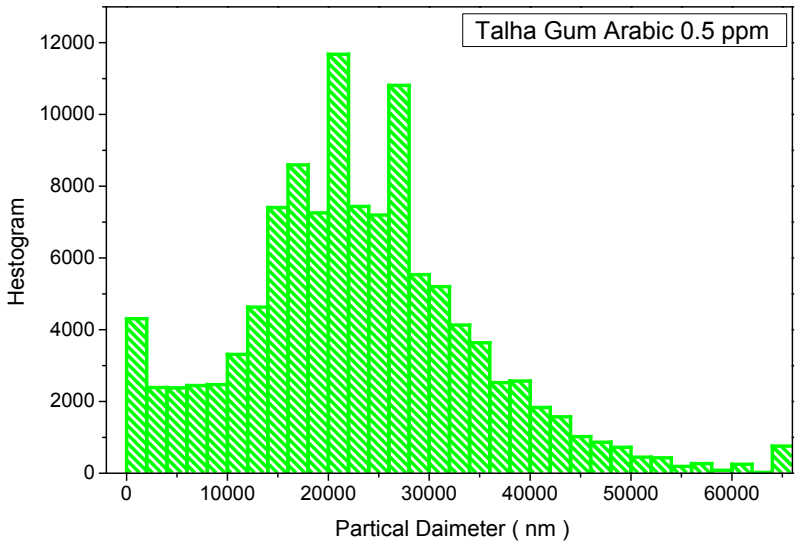

Figure (5.36) Particle diameter distribution of Talha Gum Arabic havig 0.5 ppm concentration

5.2.5 SEM Hashab Gum Arabic

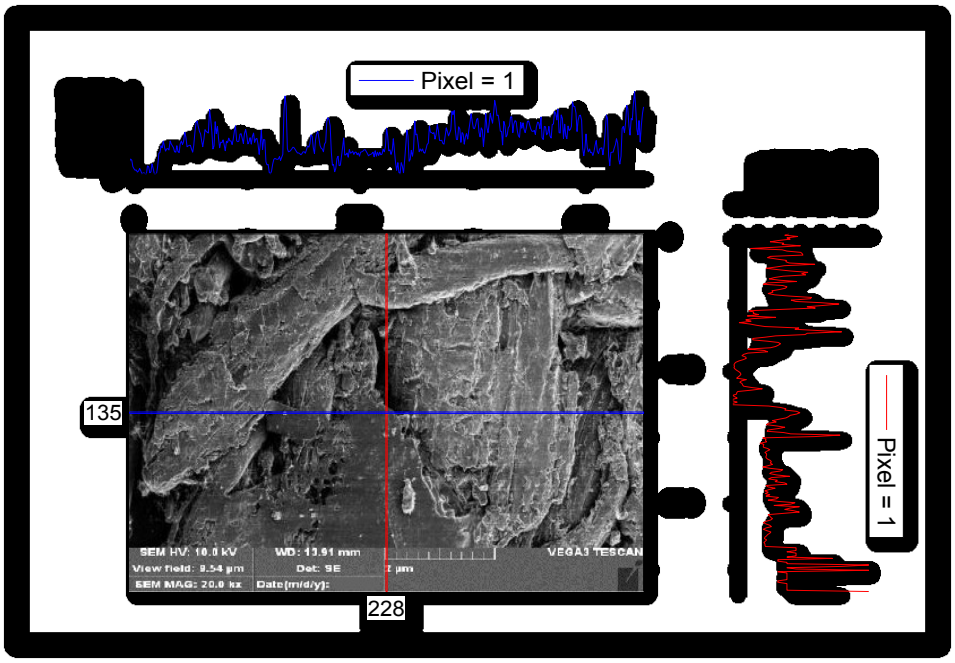

Figure (5.37) SEM images of the Hashab Gum Arabic having 0.1 ppm concentration

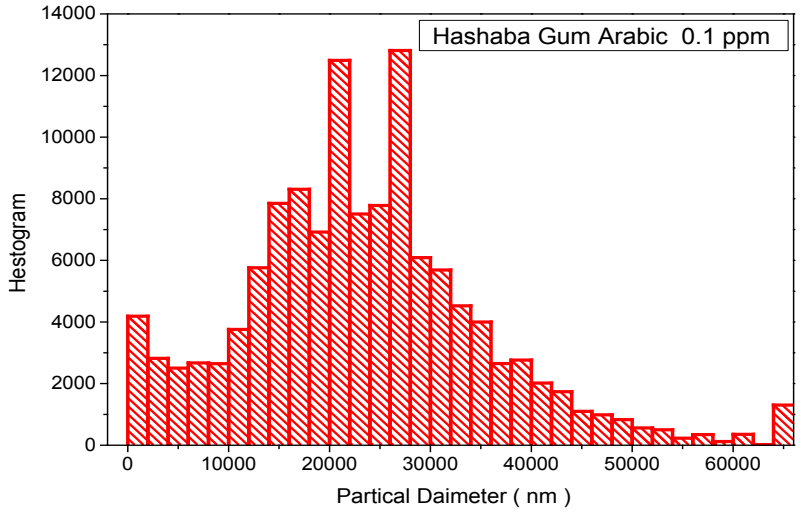

Figure (5.38) Particle diameter distribution of Hashab Gum Arabic having 0.1 ppm concentration

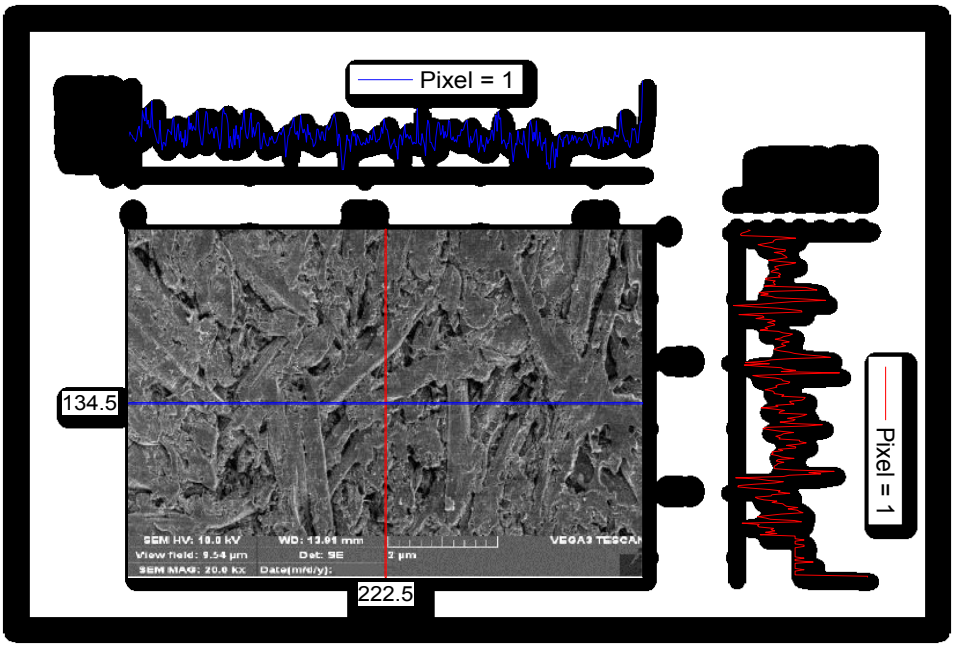

Figure (5.39) SEM images of the Hashab Gum Arabic having 0.2 ppm concentration

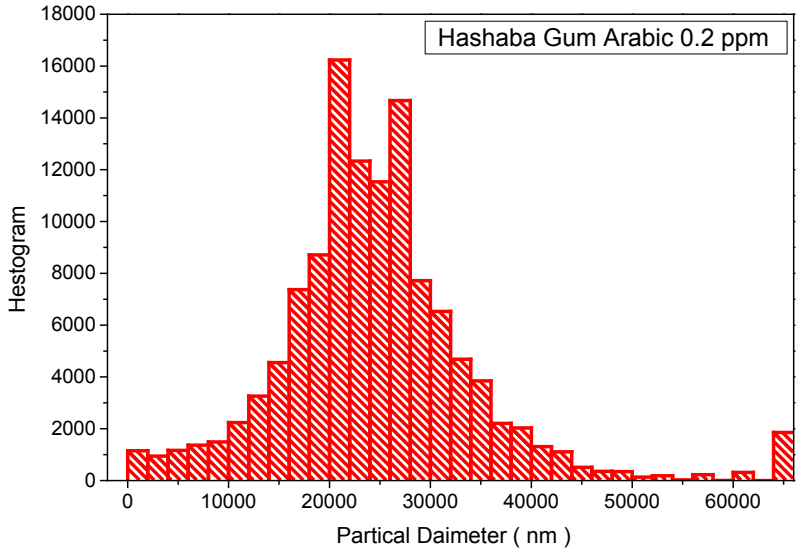

Figure (5.40) Particle diameter distribution of Hashab Gum Arabic having 0.2 ppm concentration

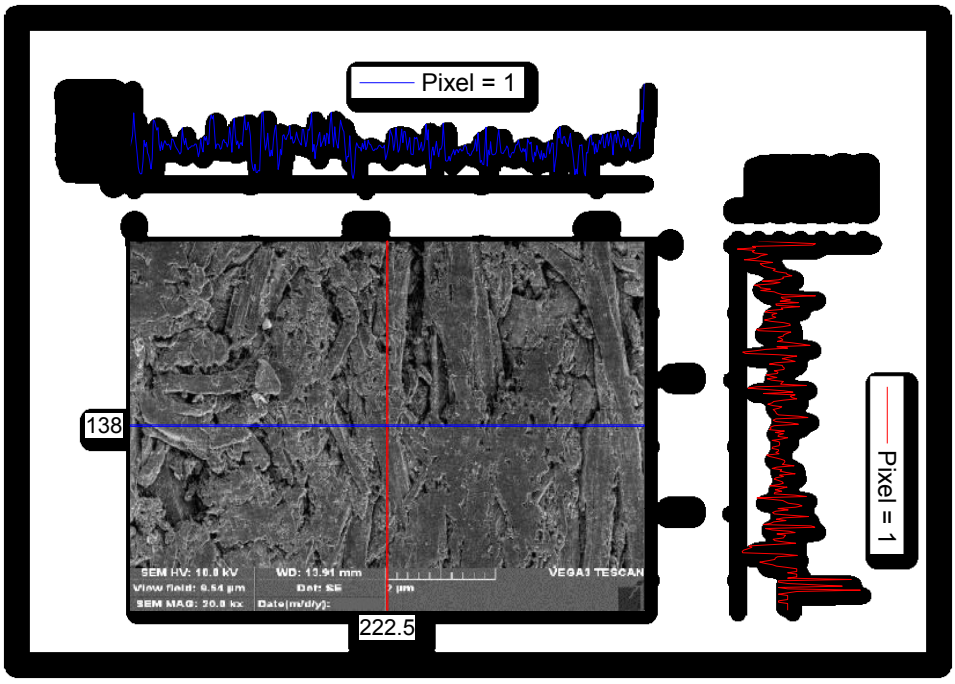

Figure (5.41) SEM images of the Hashab Gum Arabic having 0.3 ppm concentration

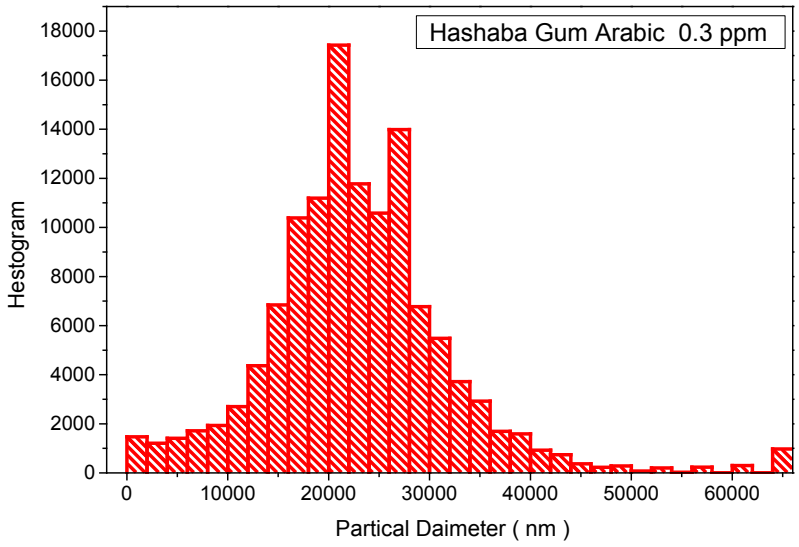

Figure (5.42) Particle diameter distribution of Hashab Gum having 0.3 ppm concentration

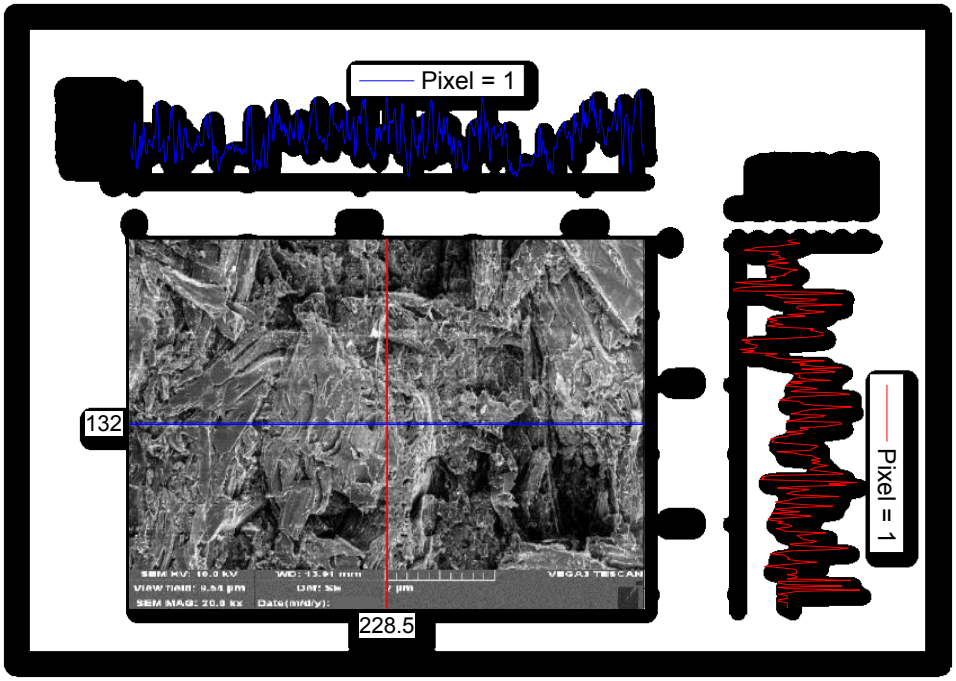

Figure (5.43) SEM images of the Hashab Gum Arabic having 0.4 ppm concentration

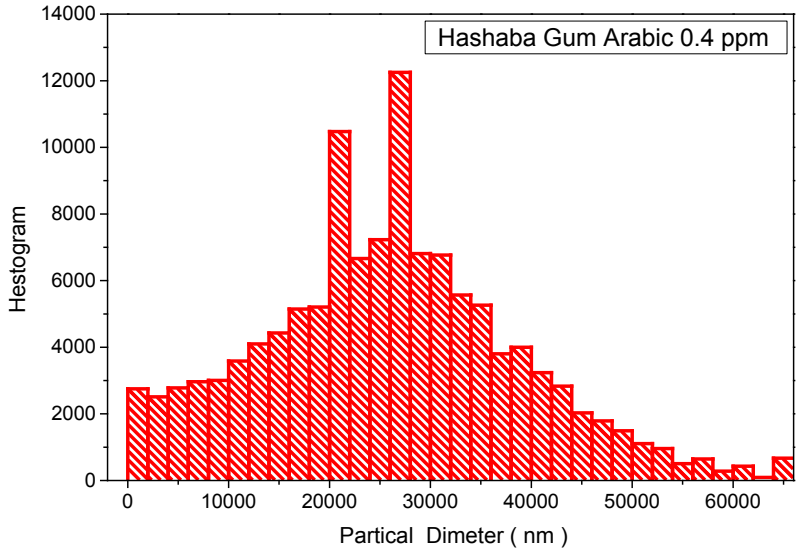

Figure (5.44) Particle diameter distribution of Hashab Gum Arabic having 0.4 ppm concentration

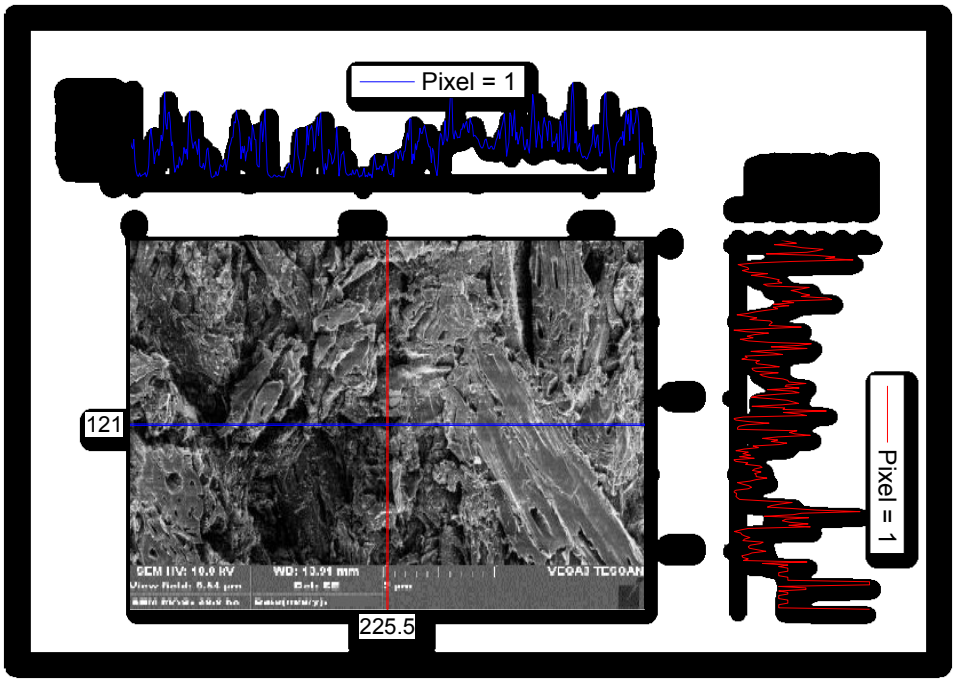

Figure (5.45) SEM images of the Hashab Gum Arabic having 0.5 ppm concentration

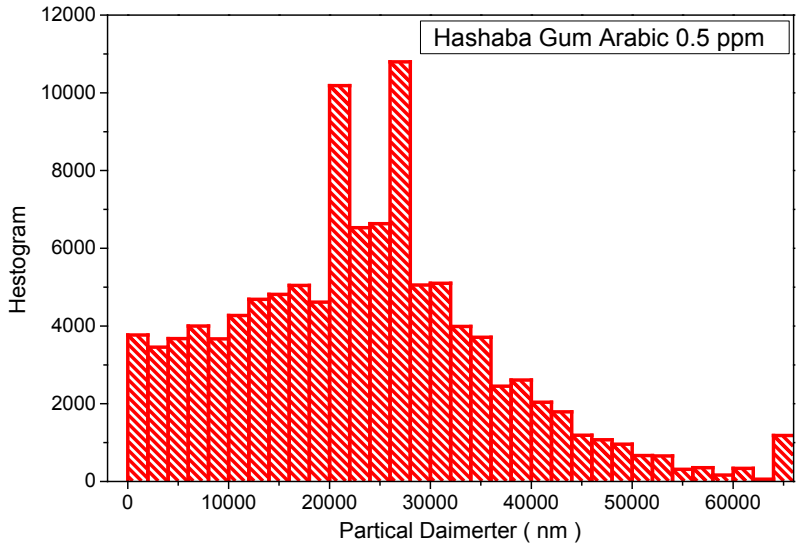

Figure (5.46) Particle diameter distribution of Hashab Gum Arabic having 0.5 ppm concentration

5.2.6 FTIR Talha Gum Arabic Results

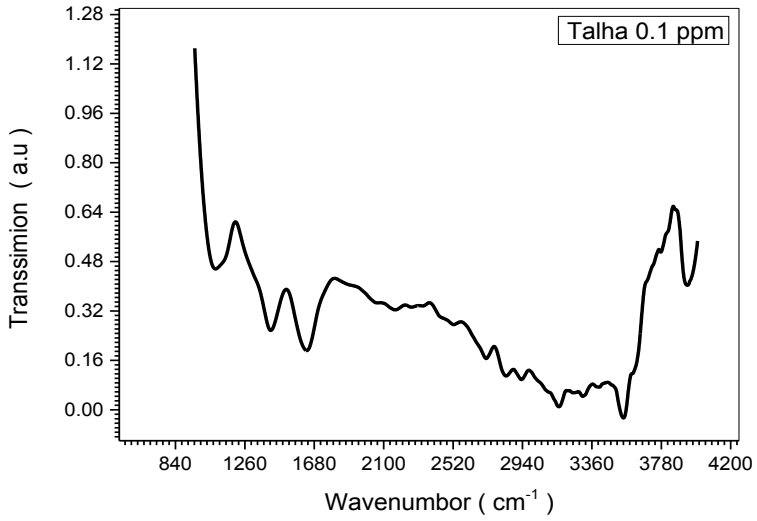

Figure (5.47) The FT-IR spectrum of Talha Gum Arabic having 0.1 ppm

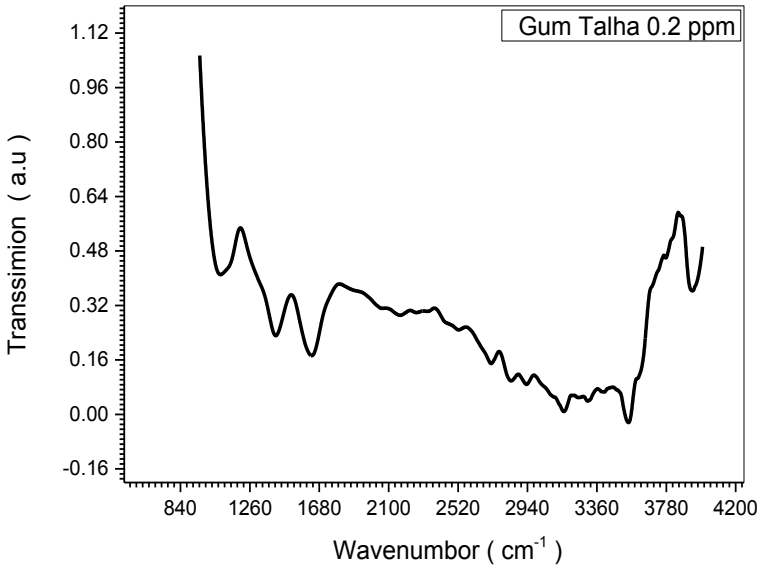

concentration

Figure (5.48) The FT-IR spectrum of Talha Gum Arabic having 0.2 ppm concentration

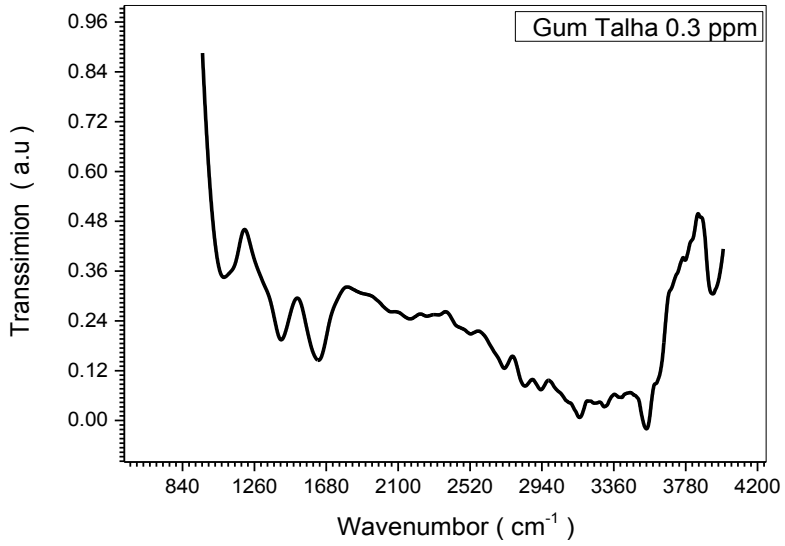

Figure (5.49) The FT-IR spectrum of Talha Gum Arabic having 0.3 ppm concentration

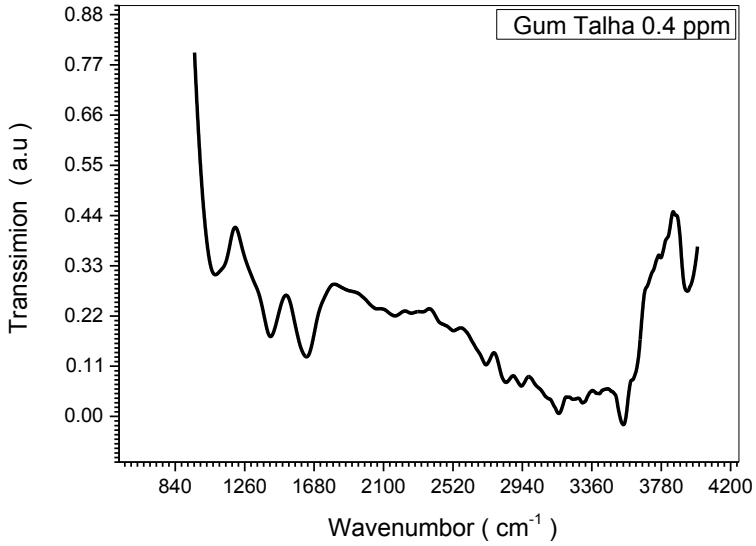

Figure (5.50) The FT-IR spectrum of Talha Gum Arabic having 0.4 ppm concentration

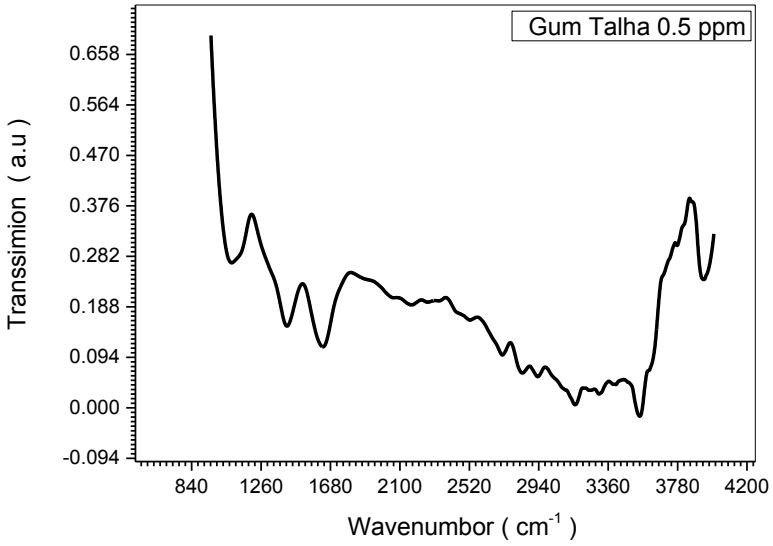

Figure (5.51) The FT-IR spectrum of Talha Gum Arabic having 0.5 ppm concentration

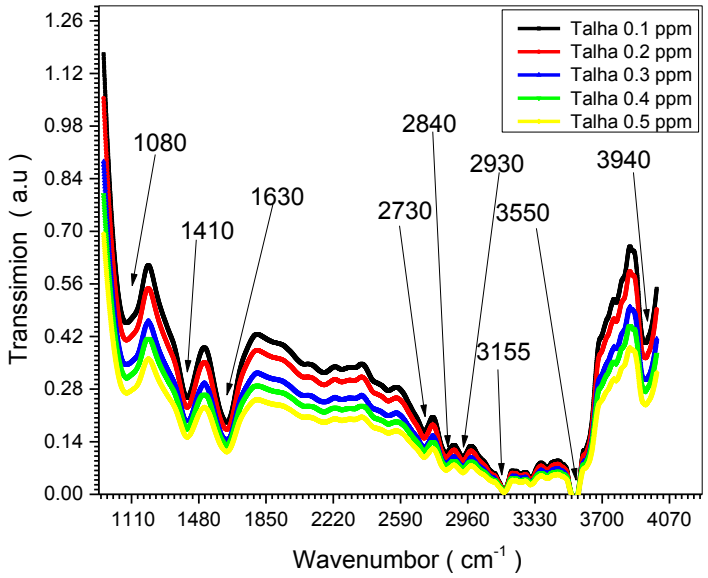

Figure (5.52) The FT-IR spectrum of five samples Talha Gum Arabic having (0.1 ,0.2 ,0.3 ,0.4 and 0.5) ppm concentration

5.2.6.1 FTIR Talha Gum Arabic Discussion

The infrared spectra of synthesized TalhaGum Arabic nano (0.1 , 0.2 ,0.3 ,0.4 and 0.5) ppm concentration were recorded by mattson Fourier Transform Infrared Spectrophotometer in the range of (500 to 4250)cm^{-1} which shown in Fig(5.47) to (5.51). The spectra of all samples have been used to locate the band positions which are given in the Table(5.2) In the present study the absorption bands ν_1 ,ν_2 ,ν_3 ,ν_4 ,ν_5 ,ν_6 ,ν_7 ,ν_8 and ν_9 are found to be around (1080 ,1410 ,1630 ,2730 , 2840 , 2930 , 3155 ,3550 and 3940) cm^{-1}respectively for all the compositions. The transmiattance bands within these specific limits reveal the formation of single-phase spinel structure having sub-lattices tetrahedral (B). The band (ν_1) around 1080 cm^{-1} is due to alkolxy C-O .The band (ν_2) around 1410 cm^{-1} is associated with the O-H bending vibration. The band (ν_3) around 1630cm^{-1} is due to C=C stretching. The band (ν_4) , (ν_5) (ν_6) around (2730 , 2840 and 2930) cm^{-1} due to C-H alkan . For (ν_7, ν_8 and ν_9) around (3155 ,3550 and 3940)cm^{-1} is due to the stretching mode of H-O-H bending vibration of free or absorbed water which implies that the hydroxyl groups are retained in ferrites .

Table (5.2) parameters of Talha Gum Arabic Nano samples

No.	**Compounds**	$\boldsymbol{v_1}$	$\boldsymbol{v_2}$	$\boldsymbol{v_3}$	$\boldsymbol{v_4}$	$\boldsymbol{v_5}$	$\boldsymbol{v_6}$	$\boldsymbol{v_7}$	$\boldsymbol{v_8}$	$\boldsymbol{v_9}$	**Bonding type**
1	Talha Gum 0.1 ppm	1080	1410	1630	2730	2840	2930	3155	3550	3940	C-O,O-H, C=C, C-H , C-H,C-H, H-O-H,H-O-H, H-O-H
2	Talha Gum 0.2ppm	1080	1410	1630	2730	2840	2930	3155	3550	3940	C-O,O-H, C=C, C-H , C-H,C-H, H-O-H,H-O-H, H-O-H
3	Talha Gum 0.3 ppm	1080	1410	1630	2730	2840	2930	3155	3550	3940	C-O,O-H, C=C, C-H , C-H,C-H, H-O-H,H-O-H,H-O-H
4	Talha Gum 0.4 ppm	1080	1410	1630	2730	2840	2930	3155	3550	3940	C-O,O-H, C=C, C-H , C-H,C-H, H-O-H,H-O-H,H-O-H
5	Talha Gum 0.5 ppm	1080	1410	1630	2730	2840	2930	3155	3550	3940	C-O,O-H, C=C, C-H , C-H,C-H, H-O-H,H-O-H,H-O-H

5.2.7 FTIR Hashab Gum Arabic Results

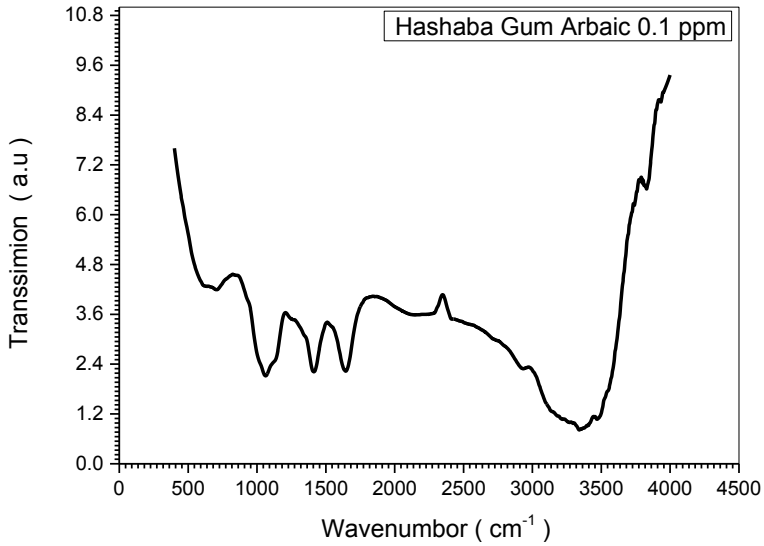

Figure (5.53) The FT-IR spectrum of Hashab Gum Arabic having 0.1 ppm concentration

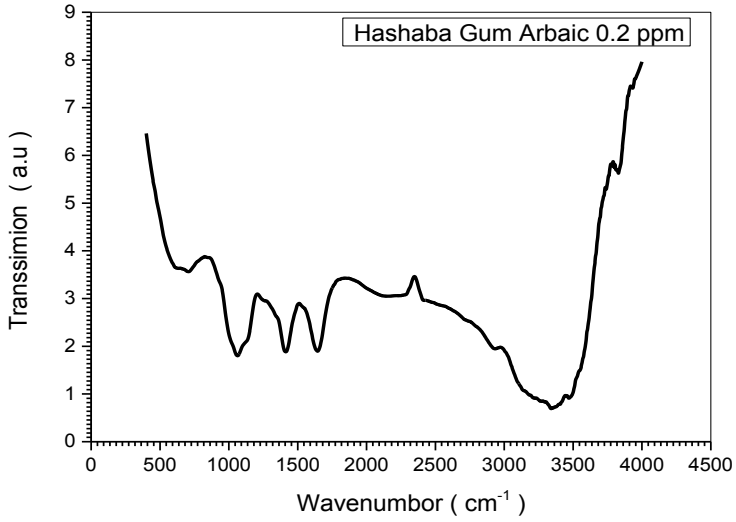

Figure (5.54) The FT-IR spectrum of Hashab Gum Arabic having 0.2 ppm concentration

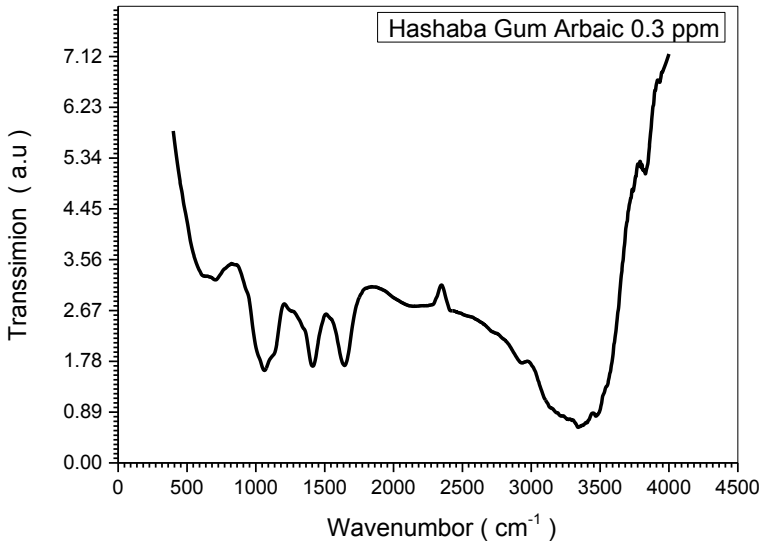

Figure (5.55) The FT-IR spectrum of Hashab Gum Arabic having 0.3 ppm concentration

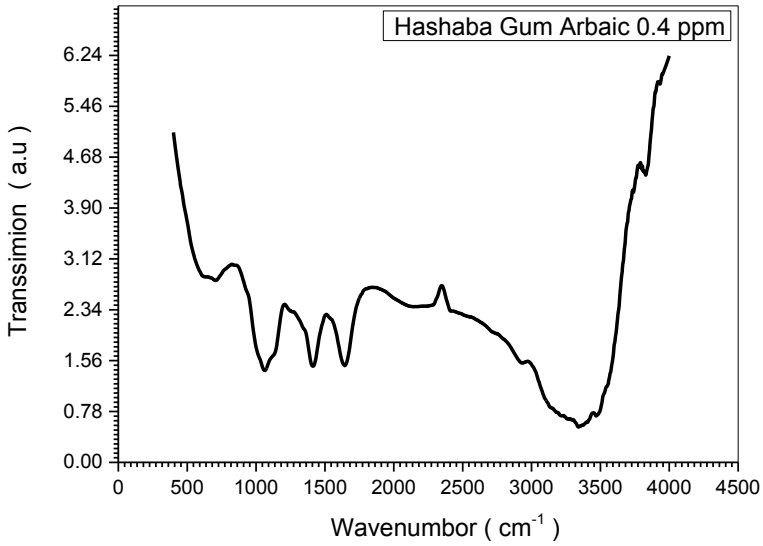

Figure (5.56) The FT-IR spectrum of Hashab Gum Arabic having 0.4 ppm concentration

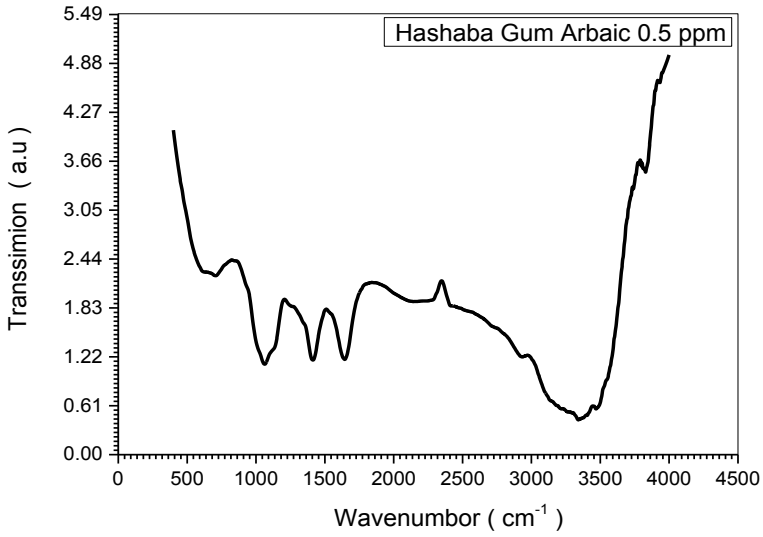

Figure (5.57) The FT-IR spectrum of Hashab Gum Arabic having 0.5 ppm concentration

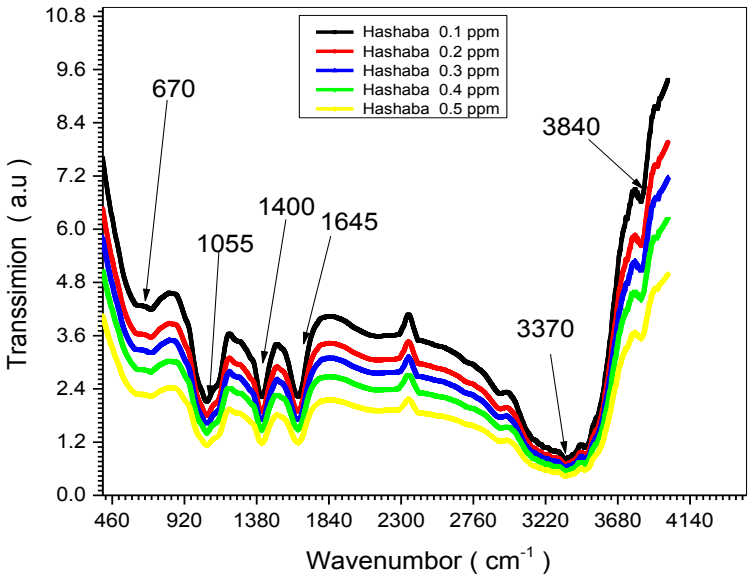

Figure (5.58) The FTIR spectrum of five samples Hashab Gum Arabic having (0.1, 0.2, 0.3, 0.4 and 0.5) ppm concentration

5.2.7.1 FTIR Hashab Gum Arabic Discussion

The infrared spectra of synthesized Hashab Gum Arabic nano (0.1 , 0.2 ,0.3 ,0.4 and 0.5) ppm concentration were recorded by mattson Fourier Transform Infrared Spectrophotometer in the range of (400 to 4500)cm^{-1} which shown in Fig(5.53) to (5.57). The spectra of all samples have been used to locate the band positions which are given in the Table (5.3) In the present study the absorption bands ν_1, ν_2, ν_3, ν_4 , ν_5, and ν_6 are found to be around (670 ,1055, 1400 ,1645 , 3370 and 3840) cm^{-1}respectively for all the compositions. The transmiattance bands within these specific limits reveal the formation of single-phase spinel structure having two sub-lattices tetrahedral (A) site and octahedral (B) site. The (ν_1) band around 670 $cm^{-1}$is caused by the metal-oxygen vibration in the tetrahedral sides. This difference in the spectral positions is due to the different values of metal ion-O^{-2} distances for octahedral and tetrahedral sites. The band (ν_2) around 1055 cm^{-1} is due to C-O stretch bending. The band (ν_3) around 1400 cm^{-1} is associated with the O-H bending vibration. The band (ν_4) around 1645cm^{-1} is due to C=C stretching. (ν_5, ν_6) around 3370 cm^{-1} and 3840 cm^{-1} is due to the stretching mode of H-O-H bending vibration of free or absorbed water which implies that the hydroxyl groups are retained in ferrites .

Table (5.3) parameters of Hashab Gum Arabic Nano samples

No.	**Compounds**	$\boldsymbol{\upsilon_1}$	$\boldsymbol{\upsilon_2}$	$\boldsymbol{\upsilon_3}$	$\boldsymbol{\upsilon_4}$	$\boldsymbol{\upsilon_5}$	$\boldsymbol{\upsilon_6}$	**Bonding type**
1	Hashab Gum 0.1 ppm	670	1055	1400	1645	3370	3840	M-O,C-O,O-H, C=C,H-O-H
2	Hashab Gum 0.2ppm	670	1055	1400	1645	3370	3840	M-O,C-O,O-H, C=C,H-O-H
3	Hashab Gum 0.3 ppm	670	1055	1400	1645	3370	3840	M-O,C-O,O-H, C=C,H-O-H C=C,H-O-H
4	Hashab Gum 0.4 ppm	670	1055	1400	1645	3370	3840	M-O,C-O,O-H, C=C,H-O-H
5	Hashab Gum 0.5 ppm	670	1055	1400	1645	3370	3840	M-O,C-O,O-H, C=C,H-O-H

5.3 Discussion

For Talha the increase of iodine concentrations increases density as shown in fig(5.3) .This conforms with fact that the crystal spacing between successive planes and unit cells decreases also as shown in fig(5.5).Because this shrinking cause atoms to be more close together and as result the density increases. The decrease of the nano crystal size x_s upon increasing iodine concentration [see figure (5.4)] also conforms with to the fact that the distance between adjacent atoms decrease due to the decrease of d-spacing. The same hold for Hashab gum, where the increase of iodine concentration increases the density [see figure (5.6)] accompanied by the decrease of nano crystal size and d-spacing as shown in figures (5.7) and (5.8) respectively.

The SEM estimated crystal sizes for Talha shown in figures(5.27-36) show a decrease in the crystal size for densities 0.1 , 0.2 , 0.3 , 0.4 ,0.5 ppm giving decreases values(98.60 , 85.52, 69.28, 60.59, and 53.46 nm) respectively. Comparing these results with that in table (5.1),it is clear that the two results are compatible to each other. The SEM crystal sizes obtained for Hashab in figures(5.37-46) indicates a decreases in the crystal size for densities 0.1 , 0.2 , 0.3 , 0.4 ,0.5 ppm giving decreased sizes(96.63 , 82.98, 76.41, 67.11, and 52.57 nm) respectively, these obtained sizes are comparable with the corresponding sizes obtained using XRD technique as shown in table(5.1).

The absorption coefficients for Talha and Hashab shown in figure (5.12) and (5.21) respectively, indicates increase of absorption coefficient upon increasing iodine concentration. This may be attributed to the fact that increase of iodine concentration increases gum density, which increases the number of atoms that absorb photons, which in turn increases absorption coefficient. The increase of iodine concentration decreases the energy gap for Talha to be (2.364, 2.356, 2.352, 2.345, and 2.339 eV).This may be due to the fact that increasing concentration increases atomic density which increases the number of states in both conduction and valance band which causes the

energy gap to be narrow. For Hashab the result is different where the increase of iodine concentration increases the energy gap to be (2.453, 2.467, 2.473, 2.482, and 2.493 eV) it also increases absorption . This may be attributed to the fact that increasing iodine concentration increases matter density which in turn increases absorption due to the increase of number of atoms.

5.4 Conclusion

The doping of Talha and Hashab gum Arabic with iodine decreases crystal spacing and nano crystal size. It increases absorption coefficient also. For Talha the energy gap decreases upon increasing iodine concentration while the energy gap increases for Hashab. This means that all studied properties of Talha and Hashab are identical except the energy gap. It is clear that Talha semiconducting behavior is better than that of Hashab .This is since the energy gap of Talha is less than that of Hashab. More over the energy gap of Talha can be decreased when doped with iodine. Increasing iodine concentration decreases the energy gap thus improving semiconducting properties.

The FTIR annoys shows some interesting properties about the types of bonding. Hashab samples show the existence of metallic bonding, while in Talha such bonding does not exist. This may explain why doping Hashab with iodine doesn't change the energy gap while iodine becomes free in Talha samples. Thus increasing iodine concentration increases free electrons which is equivalent to energy gap decrease. The number of bonds in Talha is 9, while they are only 6 in Hashab.This means that the number of bonds in Talha is more than that of Hahab. The common bonds between them are O-H , H-O-H ,C-O and C=C. The Talha has C-H bonding which does not exist in Hashab, in addition to the existence of extra H-O-H bonding in Talha. The energy of bonds which are common for them is not the same, which reflect different crystal fields and different chemical compositions. The existence of

O, H, and C confirms that our samples in an organic material like gum Arabic. The existence of metallic bond also confirms the existence of iodine.

5.5 Recommendation

1. The effect of pressing Talha and Hashab on its optical and electrical properties needs to be studied.
2. The change of optical and electrical properties when replacing iodine with other compounds should be studied also.
3. The thermal and mechanical properties of the studied samples must also studied.

References:

[1] Poole Jr, Charles P., and Frank J. Owens. *Introduction to nanotechnology*. John Wiley & Sons, Canada (2003).

[2] Bruus, Henrik. *Introduction to nanotechnology*. Department of Micro and Nanotechnology, Technical University of Denmark, (2004).

[3] Tarafdar, J. C., Shikha Sharma, and Ramesh Raliya. "Nanotechnology: Interdisciplinary science of applications." *African Journal of Biotechnology* Vol.12, No 3 (2013).

[4] Whatmore, Roger W. "Nanotechnology—what is it? Should we be worried?." *Occupational Medicine* Volume 56, Issue 5, (2006): 295-299.

[5] Gatoo, Manzoor Ahmad, et al. "Physicochemical properties of nanomaterials: implication in associated toxic manifestations." *BioMed research international* Volume 2014 (2014)

[6] Ramsden, Jeremy. *Essentials of nanotechnology*, Ventus Publishing ApS, (2009).

[7] Fiiipponi, Luisa, and Duncan Sutherland, eds. *Nanotechnologies: principles, applications, implications and hands-on activities: A compendium for educators*. European Union, Directorate General for Research and Innovation, (2012).

[8] Nouailhat, Alain. *An introduction to nanoscience and nanotechnology*. Vol. 10. John Wiley & Sons, Hoboken, USA, (2007).

[9] Bhushan, Bharat, ed. *Springer handbook of nanotechnology*. Springer, (2006).

[10] Hornyak, Gabor L., et al. *Fundamentals of nanotechnology*. CRC press, London New york (2018).

[11] Melnik, A. V., and O. V. Shagalina. "History of Nanotechnology." *Siberian Federal University* (2011).

[12] Sze, Simon Min. *Semiconductor devices: physics and technology*. John wiley & sons, (2008).

[13] Pasa, Andre A. "Chapter 13: Metal Nanolayer-Base Transistor." (2010):13-1.

[14] Tolochko, N. K. "History of nanotechnology." *Encyclopedia of Life Support Systems (EOLSS) Belarus State Agrarian Technical University, Belarus* (2009).

[15] Roco, Mihail C. "The long view of nanotechnology development: the National Nanotechnology Initiative at 10 years." *Nanotechnology research directions for societal needs in 2020*. Springer, Dordrecht, 2011.pp 1-28

[16] Brochier, Fabien. *Electricity and Magnetism*. Routledge ,(2004).

[17]http://manyet.com/en/the-importance-of-magnets-in-our-daily-lives/The Importance of Magnets in Our Daily Lives 1:48 PM

[18]https://www.thehindu.com/features/kids/Importance-of electricity/article16544961.ece Importance of electricity 1:25 PM

[19] Dror, Yael, Yachin Cohen, and Rachel Yerushalmi-Rozen. "Structure of gum arabic in aqueous solution." *Journal of Polymer Science Part B: Polymer Physics* Volume 44, Issue22 (2006): 3265-3271.

[20] Ahmed, Abdelkareem A. "Health benefits of gum arabic and medical use." *Gum Arabic*. Academic Press(2018). P. 183-210

[21]Grein, Aline,etal. "Structural characterization and emulsifying properties of polysaccharides of Acacia mearnsii de Wild gum." *Carbohydrate polymers* Volume 92, Issue1 (2013):PP. 312-320.

[22] Montenegro, Mariana A., et al. "Gum Arabic: More Than an Edible Emulsifier Products and Applications of Biopolymers, Dr." Edited by Dr. Johan Verbeek, Publisher In Tech." (2012).

[23] Sears, Francis W., Mark W. Zemansky, and Hugh D. Young. " University physics. Addison." (1987).

[24] Cutnell, John D., and Kenneth W. Johnson. "Physics Fifth Edition." John Wiley and Son, (2001).

[25]Shackelford, James F. "Materials science for engineers." *River, New Jersey* (2000).

[26] Ebnouf , Zohl. "Optical properties of Nano-Crystalline Zn Fluorescein Thin Films." Ph.D.(2019).

[27] Fox, Mark. "Optical properties of solids." Published in the United States (1970).

[28] Ahmed, Abdel Fattah. "Solid state physics." volume Three

[29] Kant, Rajni. "Applied Solid State Physics. " John Wiley & Sons, India (2013).

[30]Hofmann, Philip. "*Solid state physics: an introduction*. " John Wiley & Sons- VCH Verlag GmbH (2015).

[31] Ibach, H., and H. Luth. "Solid-State Physics: An Introduction "to Principles of Materials Science, (2002).

[32] Ling, Samual J., et al. "University Physics Volume 2." Houston (2016).

[33] Halliday, David, Robert Resnick, and Jearl Walker. *Fundamentals of physics*. John Wiley & Sons, USA(2013).

[34] Serway, Raymond A., and Larry D. Kirkpatrick. "Physics for scientists and engineers with modern physics." (1988): 254-255.

[35] Serway, Raymond A., and Chris Vuille. *College physics*. Nelson Education (2014).

[36] Keer, Hemant V. *Principles of the solid state*. New Age International (1993).

[37] Bishop, Chris. "The relationship between loss, conductivity, and dielectric constant." *Adv. Eng. Electromagn* (2001).

[38] Alonso, Marcelo, and Edward J. Finn. "Physics Addison-Wesley." *Wokingham, England* (1992).

[39]Buzea, Cristina, Ivan I. Pacheco, and Kevin Robbie. "Nanomaterials and nanoparticles: sources and toxicity." Biointerphases Vol.2, Issue 4 (2007): MR17- MR71.

[40] Hong, Nguyen Hoa. "Introduction to nanomaterials: basic properties, synthesis, and characterization." *Nano-Sized Multifunctional Materials*. Elsevier,(2019).P. 1-19.

[41]Petit, Christophe, Patricia Lixon, and Marie Paule Pileni. "In situ synthesis of silver nanocluster in AOT reverse micelles." *The Journal of Physical Chemistry* 97.49 (1993): 12974-12983.

[42] Jeevanandam, Jaison, et al. "Review on nanoparticles and nanostructured materials: history, sources, toxicity and regulations." Beilstein journal of nanotechnology 9.1 (2018): 1050-1074.

[43] Oberdörster, Eva, et al. "Ecotoxicology of carbon-based engineered nanoparticles: effects of fullerene (C60) on aquatic organisms." *Carbon Vol* 44.Issue 6 (2006): PP. 1112-1120.

[44] Dreizin, Edward L. "Metal-based reactive nanomaterials." *Progress in energy and combustion science* Vol35, Issue2 (2009): PP.141-167.

[45] Astruc, Didier, Elodie Boisselier, and Catia Ornelas. "Dendrimers designed for functions: from physical, photophysical, and supramolecular properties to applications in sensing, catalysis, molecular electronics, photonics, and nanomedicine." *Chemical reviews* 110.4 (2010): 1857-1959.

[46] Schadler, Linda S., and Paul V. Braun. *Nanocomposite science and technology*. Wiley VCH, (2002).

[47] Christian, P., et al. "Nanoparticles: structure, properties, preparation and behaviour in environmental media." *Ecotoxicology* 17.5 (2008): 326-343

[48] Borm, Paul JA, et al. "The potential risks of nanomaterials: a review carried out for ECETOC." *Particle and fibre toxicology* 3.1 (2006): 1-35.

[49]Holister, Paul, et al. "Nanoparticles." *Technology white papers* 3, Cientifica (2003):P.1-11.

[50]Robbie, K., et al. "Designed Nanoparticles." (2007).

[51]Anderson, D. M. W., J. R. A. Millar, and Wang Weiping. "Gum Arabic (Acacia senegal) from Níger-Comparison with other sources and potential agro forestry development." *Biochemical systematics and ecology* Vol.19.Issue 6 (1991): PP.447- 452.

[52] Lelon, J. K., et al. "Influence of Acacia senegal varieties on quality of gum arabic in Baringo District Kenya." *African Journal of Plant Science* 7.6 (2013): 190-200.

[53] Anurag, Tewari. "An over view on chemistry and applications of acacia gums." *Der Pharma Chemica* 2.6 (2010): 327-331.

[54]P.A. and G.O. North East Wales Institute, Wrexham (1990)

[55] Mokhtar, Leila. "Electric conductivity of gum Arabic from Acacia senegal." medicine 1 (2013): 2.

[56] Anderson, D. M. W., J. F. Howlett, and C. G. A. McNab. "The amino acid composition of the proteinaceous component of gum karaya (Sterculia spp.)." *Food Additives& Contaminants* Vol.2, Issue3 (1985):PP. 153-157

[57] Erskine, A. J., and J. K. N. Jones. "Fractionation of polysaccharides." *Canadian Journal of Chemistry* Vol.34, No. 6 (1956): 821-826.

[58] Anderson, D. M. W., and I. C. M. Dea. "Studies on uronic acid materials: Part XXV. Some unusual forms of the gum from Acacia senegal willd." *Carbohydrate Research* Vol6, Issue1 (1968): pp.104-110.

[59]Rosenfeld, Louis. "Discovery and early uses of iodine." *Journal of Chemical Education* 77.8 (2000): 984.

[60] Cooper, Rose A. "Iodine revisited." *International wound journal* Vol.4, Issue 2 (2007): PP. 124-137

[61] Lyday, Phyllis A., and Tatsuo Kaiho. "Iodine and iodine compounds." *Ullmann's Encyclopedia of Industrial Chemistry* (2000): PP.1-13.

[62] Zhdankin, Viktor V. *Hypervalent iodine chemistry: preparation, structure and synthetic applications of polyvalent iodine compounds*. John Wiley & Sons, 2013.

[63] Sparks, Donald L., and Donald L. Sparks. *Advances In Agronomy Vol.- . 87*. Elsevier, 2005

[64] RĂPUNTEAN, Sorin, et al. "The effect of iodine based products on unicellular algae from genus Prototheca." *Bulletin of the University of Agricultural Sciences & Veterinary Medicine Cluj-Napoca. Veterinary Medicine* 72.2 (2015).

[65] Atkins, Peter, and Loretta Jones. *Chemical principles: The quest for insight*. Macmillan, (2007).

[66] Braner, A. A., and R. Chen. "Some optical properties of iodine single crystals." *Journal of Physics and Chemistry of Solids* 24.1 (1963): 135-139.

[67] Kaiho, Tatsuo, ed. *Iodine chemistry and applications*. John Wiley & Sons, Incorporated, (2014).

[68] H. Mustafa, R.Abd Elgani, A. Suliman, A.M.Ahmed[4], Amal A.Abdallah[5], Asma Mohammed & Sawsan Ahmed Elhouri Ahmed- "*Improving the Properties of Gum Arabic to act As Semiconductor*" – Global Journal of Engineering and Researches Vol. 2(11) (2015).

[69] Kafi, Siddig T., Murwan K. Sabahalkhair, and Khartoum SUDAN. "Effects of γ-irradiation on some properties of gum arabic (Acacia senegal (*Acacia Senegal* L)." *Research Journal of Agriculture and Biological Sciences* 6.2 (2010): 113-117.

[70] Elzain, E. M. I., L. M. Mobarak, and M. Dirar. "Investigating the electric conductivity, magnetic inductivity, and optical properties of gum Arabic crystals." *J. Basic Appl. Chem* 2.6 (2012): 35-49.

[71] Lelon, J. K., et al. "Assessment of physical properties of gum arabic from Acacia senegal varieties in Baringo District, Kenya." *African Journal of Plant Science* Vol. 4(4) , (2010):PP. 95-98.

[72] Solomon, Moses M., et al. "Gum Arabic-silver nanoparticles composite as a green anticorrosive formulation for steel corrosion in strong acid media." *Carbohydrate polymers* 181 (2018): 43-55.

[73] Elliott, S. L., R. F. Broom, and C. J. Humphreys. "Dopant profiling with the scanning electron microscope—A study of Si." *Journal of applied physics* Vol. 91, No.11 (2002): 9116-9122.

[74] López-Franco, Yolanda L., et al. "Classification and physicochemical characterization of mesquite gum (Prosopis spp.)." *Food hydrocolloids* Vol.26.1 (2012):PP. 159-166.

[75] Bhakat, D., P. Barik, and A. Bhattacharjee. "Electrical conductivity behavior of Gum Arabic biopolymer-Fe3O4 nanocomposites." *Journal of Physics and Chemistry of Solids* 112 (2018):PP. 73-79.

[76] MOHAMED, ELKHATEM ELMHDY ALI. *Determination of the Energy Gap of Gum Arabic Doped with Zinc Oxide Using the UV-VIS Technique*. Diss. Sudan University of Science and Technology, 2018.

[77] Palma, Susana ICJ, et al. "Covalent coupling of gum arabic onto superparamagnetic iron oxide nanoparticles for MRI cell labeling: physicochemical and in vitro characterization." *Contrast media & molecular imaging* Vol.10, Issue 4 (2015): PP. 320-328.

[78] Barik, Puspendu, Ashis Bhattacharjee, and Madhusudan Roy. "Preparation, characterization and electrical study of gum arabic /ZnO

nanocomposites." *Bulletin of Materials Science* Vol.38, No.6 (2015): PP. 1609-1616.

[79] Pleger, Thomas C. "A brief introduction to the old copper complex of the Western Great Lakes: 4000-1000 BC." *Proceedings of the Twenty-seventh Annual Meeting of the Forest History Association of Wisconsin, Oconto, WI*. Vol. 5 (2002).

[80] Mohamed, Mohamed Azuwa, et al. "Fourier transform infrared (FTIR)
[80] spectroscopy." *Membrane Characterization*. Elsevier,(2017)PP. 3-29.

[81] Inkson, B. J. "Scanning electron microscopy (SEM) and transmission electron microscopy (TEM) for materials characterization." *Materials characterization using nondestructive evaluation (NDE) methods*. Woodhead Publishing, (2016). PP.17-43.

[82]Kuo, John, ed. *Electron microscopy: methods and protocols*. Vol. 369. Springer Science & Business Media,(2007).

[83] Vernon-Parry, K. D. "Scanning electron microscopy: an introduction." *III-Vs Review* Vol.13, Issue 4 (2000): PP.40-44.

[84] Stokes, Debbie. *Principles and practice of variable pressure/environmental scanning electron microscopy (VP-ESEM)*. John Wiley & Sons, (2008).